Journal of Medicinal Chemistry

Article

pubs.acs.org/jmc

Rational Design of Partial Agonists for the Muscarinic M_1 Acetylcholine Receptor

Xinyu Chen,[†,‡] Jessika Klöckner,[†] Janine Holze,[§] Cornelia Zimmermann,[§] Wiebke K. Seemann,[∥] Ramona Schrage,[§] Andreas Bock,[⊥] Klaus Mohr,[§] Christian Tränkle,*[,§] Ulrike Holzgrabe,*[,†] and Michael Decker*[,†,‡]

[†]Institute of Pharmacy and Food Chemistry, University of Würzburg, Am Hubland, 97074 Würzburg, Germany

[‡]Institute of Pharmacy, University of Regensburg, Universitätsstrasse 31, 93053 Regensburg, Germany

[§]Pharmacology and Toxicology Section, Institute of Pharmacy, University of Bonn, Gerhard-Domagk-Strasse 3, 53121 Bonn, Germany

[∥]Department of Pharmacology, University of Cologne, Gleueler Strasse 24, 50931 Cologne, Germany

[⊥]Institute of Pharmacology and Toxicology, University of Würzburg, Versbacher Strasse 9, 97078 Würzburg, Germany

Supporting Information

ABSTRACT: Aiming to design partial agonists for a G-protein-coupled receptor based on dynamic ligand binding, we synthesized three different series of bipharmacophoric ligands composed of the orthosteric building blocks iperoxo and **1** linked to allosteric modulators (BQCA-derived compounds, BQCAd; TBPB-derived compound, TBPBd). Their interactions were studied with the human muscarinic acetylcholine M_1-receptor (hM_1) with respect to receptor binding and G_q-protein signaling. Results demonstrate that iperoxo/BQCAd (**2**, **3**) and **1**/BQCAd hybrids (**4**) act as M_1 partial agonists, whereas **1**/TBPBd hybrids (**5**) did not activate M_1-receptors. Among the iperoxo/BQCAd-hybrids, spacer length *in conjunction* with the pattern of substitution tuned efficacy. Most interestingly, a model of dynamic ligand binding revealed that the spacer length of **2a** and **3a** controlled the probability of switch between the *inactive* purely allosteric and the *active* bitopic orthosteric/allosteric binding pose. In summary, dynamic ligand binding can be exploited in M_1 receptors to design partial agonists with graded efficacy.

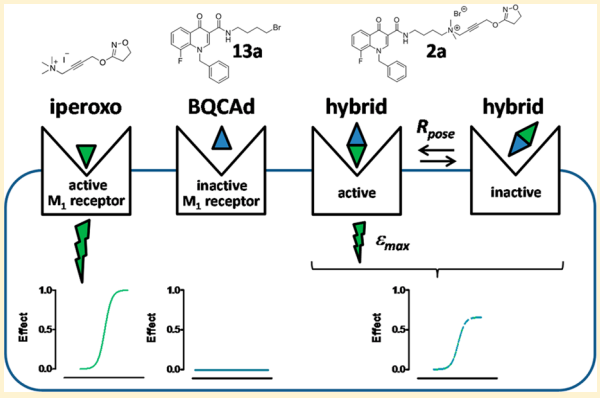

INTRODUCTION

Recently, dualsteric (bitopic orthosteric/allosteric) ligands of G protein-coupled receptors (GPCRs) have attracted much interest not only as pharmacological tools for the elucidation of receptor activation-induced conformational transitions but also as a concept for the design of new drugs.[1,2] Dualsteric compounds composed of an orthosteric ligand (either agonist or antagonist) and an allosteric moiety have been found to substantially enhance the affinity to the receptor[3] but may as well reduce affinity or leave it unchanged depending on the individual building blocks.[1] Additionally, the dualsteric approach may generate receptor subtype selectivity[4] and biased signaling.[5−7] The five M receptor subtypes ($mAChR_{1-5}$ or M_1-M_5) are metabotropic GPCRs, with M_1 being most abundantly expressed in the central nervous system (cortex, striatum, and hippocampus).[8] M_1 signaling is mediated preferentially by G_q/G_{11}-proteins activating phospholipase C and via other G-proteins initiating additional signaling systems.[9,10] Furthermore, the M_1 receptor influences ion channels that possess high relevance for cognition such as voltage-gated Ca^{2+} channels and the *N*-methyl-D-aspartate (NMDA) receptor.[11,12] Agonists of the hM_1 receptor might have therapeutic relevance because they appear to improve symptoms of schizophrenia and impaired cognitive functions such as in Alzheimer's disease (AD) as well as to positively influence other AD-related pathophysiological processes.[2,10,13−15]

The aim of this study was to design rationally as a proof-of-concept bipharmacophoric partial agonists with affinity for the M_1 receptor in three different series of hybrids and to elucidate their signaling behavior qualitatively. Signaling behavior might be of particular relevance because M_1 stimulation is considered to have more than symptomatic procognitive effects in AD[15] in that it influences pathophysiology by reducing β-amyloid 42 ($A\beta_{42}$).[10,13]

Two subtypes of muscarinic receptors are structurally well characterized by means of their crystal structures, i.e., the tiotropium-bound M_3 receptor[16] and the quinuclidinyl benzilate (QNB)-occupied M_2 receptor,[17] both captured in their inactive conformations. Very recently, the M_2 receptor has

Received: June 7, 2014

 © XXXX American Chemical Society dx.doi.org/10.1021/jm500860w | *J. Med. Chem.* XXXX, XXX, XXX−XXX

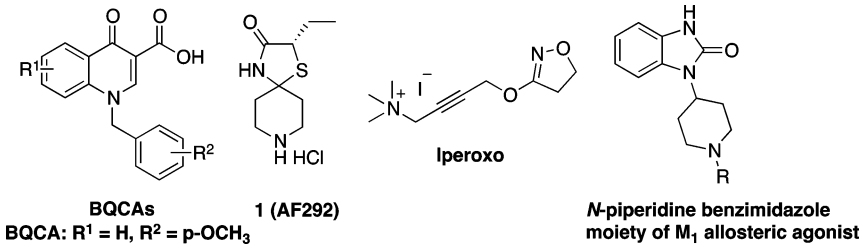

Figure 1. Structures of compounds aimed at targeting orthosteric or allosteric sites of the M_1 receptor (R = 1-(2-methylbenzyl)piperidin-4-yl for TBPB).

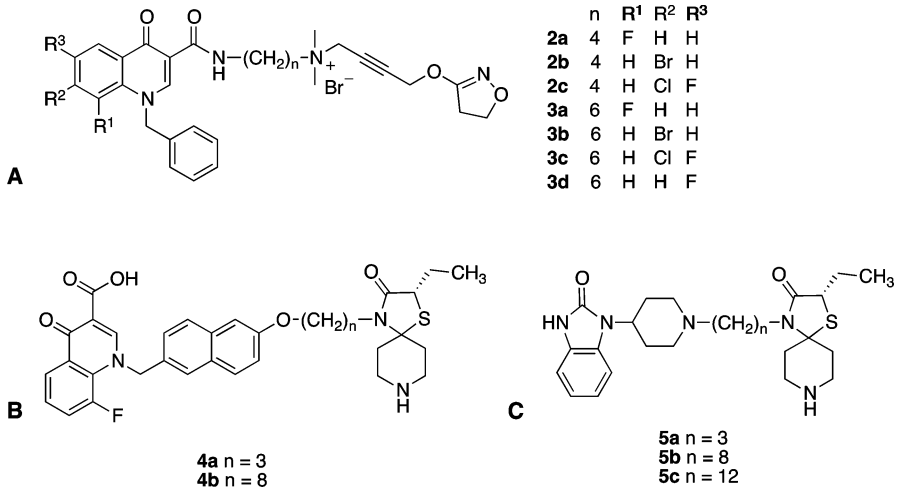

Figure 2. (A) Iperoxo/BQCAd hybrids composed of derivatives of the prototypical M_1-selective BQCA, spacer, and the M_2-superagonist iperoxo. (B) **1**/BQCAd hybrids consisting of compound **1** and a BQCA analogue. (C) **1**/TBPBd hybrids composed of compound **1** and *N*-piperidine benzimidazolone derivative.

been cocrystallized with iperoxo in the active receptor conformation.[18] Iperoxo represents a muscarinic agonist with supraphysiological efficacy at this subtype.[19] These muscarinic receptor subtypes exhibit a high structural similarity consisting of a deeply buried orthosteric binding site for agonists and antagonists connected with a allosteric vestibule formed by solvent accessible extracellular loops and the extracellular parts of transmembrane helices (TM) 3, 5, and 7. These features also apply to other class A receptors.[20] Because of the sequence identity between M_1 and M_3 receptors and M_1 and M_2 subtypes amounting to 49.7 and 45.0%,[21] respectively, Ilien et al. were able to develop a valid homology model of the M_1 receptor.[22,23] Using this model, they could characterize the bitopic behavior of hybrid ligands composed of the M_1-selective antagonist pirenzepine and the allosteric fluorescent label Bodipy; these two moieties were connected via an alkylene, polyethylene glycol, or amidoalkylene linker.

The orthosteric binding site of muscarinic receptors is well characterized by computational and molecular biology methods (for reviews see Davie 2013 and Goodwin 2007),[2,24] unraveling the essential role of a negatively charged aspartate residue in TM3 that interacts with the positively charged nitrogen of the endogenous ligand acetylcholine or antagonists like protonated atropine.[16,17] Currently, the presence of more than one allosteric binding site is discussed: the "common allosteric site" relates to the above-mentioned allosteric vestibule being located next to the aforementioned extracellular loops (ECL2 and 3; vestibule) including negatively charged residues in ECL3. The topography of this site is conserved across the subtypes. Because of their positive charges, archetypal modulators such as alcuronium and gallamine bind to the common allosteric site.[25,26] In addition, a second allosteric binding site was postulated which seems to be occupied by the compounds (9*S*,10*S*,12*R*)-2,3,9,10,11,12-hexahydro-10-hydroxy-9-methyl-1-oxo-9,12-epoxy-1*H*-diindolo[1,2,3-*fg*:3′,2′,1′-*kl*]pyrrolo[3,4-*i*][1,6]benzodiazocine-10-carboxylic acid hexyl ester (KT5720)[27] and 17-β-hydroxy-17-α-ethynyl-δ-4-androstano[3,2-*b*]pyrimido[1,2-*a*]benzimidazole (WIN62,577).[28]

By designing bipharmacophoric ligands consisting of the M_2-superagonist iperoxo[19] and a phthalimido- or naphthalimido-propylammonium moiety, which were found to bind to M_2 receptors with moderate selectivity, we had learned that subtype selectivity of ligand binding can be achieved by concomitantly addressing the allosteric and orthosteric site.[29] Compared to conventional agonists, including acetylcholine, these ligands are able to preferentially use one signaling pathway over others, hence displaying biased signaling.[4,5] In addition and most interestingly with respect to the current study, receptor binding of a bipharmacophoric compound may theoretically switch between a dualsteric and a purely allosteric orientation.[4,7,30] Regarding bipharmacophoric M_2 receptor ligands, the dynamic switch between dualsteric active and allosteric inactive binding orientations (R_{pose}) has recently been employed for the rational design of partial agonists.[30] Partial agonist activity could be a beneficial feature of potential M_1 selective anti-Alzheimer drugs because it is known that partial agonism can reduce agonist-induced receptor desensitization.[31] Furthermore, partial agonism is a currently debated concept in the design of new antipsychotic GPCR drugs.[32]

dx.doi.org/10.1021/jm500860w | J. Med. Chem. XXXX, XXX, XXX−XXX

Scheme 1. Synthesis of Iperoxo/BQCAd Hybrids[a]

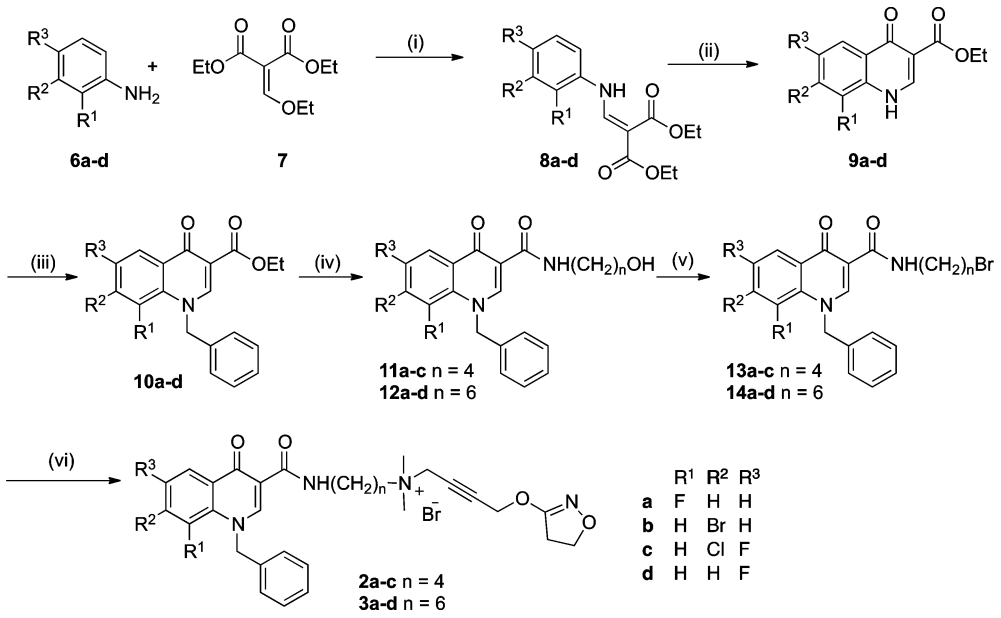

[a]Reagents and conditions: (i) toluene, reflux; (ii) diphenyl ether, 210 °C (microwave); (iii) benzyl chloride, K_2CO_3, DMF, 80 °C, 72%; (iv) $H_2N(CH_2)_nOH$, 130−150 °C, 57%; (v) HBr, H_2SO_4, reflux, 50%; (vi) iperoxo base, K_2CO_3, CH_3CN, 55 °C, 44%.

In the current study, we synthesized derivatives of highly subtype selective allosteric ligands and linked them to orthosteric agonists aiming to design bipharmacophoric M_1 receptor agonists. From the group of allosteric M_1 ligands developed by different companies such as Acadia, Merck, Lundbeck, or research institutes and groups like Vanderbilt University, Christopoulos, and others,[2,10,33,34] we have chosen the benzyl quinolone carboxylic acids (BQCAs), being a group of ligands with positive allosteric modulator (PAM) properties with respect to agonist (not antagonist) binding and function in M_1 receptors.[34−37] Additionally, BQCA has been shown to have allosteric agonist properties.[34,38] Recently, we applied the message-address concept successfully to the design of dualsteric M_2 ligands which displayed G_i biased signaling.[4,5] In the current study, following a similar approach, derivatives of the prototypal M_1 selective BQCA (BQCAd) served as the M_1 address which was linked via a spacer to an agonist, either compound **1** (AF292), which is claimed to be a M_1 selective agonist,[39] or the orthosteric M_2-superagonist iperoxo (Figure 1).[19] Two points of attachment were chosen due to the structure−activity relationships (SARs) reported in the literature:[40] the carboxylic group and the benzyl group. Because the carboxylic group is a suitable contact point for improving allosteric modulation, we herewith describe the synthesis of iperoxo/BQCAd-prototype hybrids (**2**,**3**) utilizing the carboxylic functional group to connect the spacer (Figure 2A). Of note, that these quarternary compounds (**2**,**3**) are unlikely to penetrate the blood−brain barrier and were not designed in an attempt to perform drug development but as a proof-of-concept regarding bipharmacophoric partial M_1 agonists. Furthermore, the M_1 agonist **1**[39,41] was attached to the naphthalene residue of a BQCA-derived compound (**4**, Figure 2B). With regard to compound **1**, the lactam nitrogen atom was chosen for connection because its modification seemed the least susceptible to a loss of affinity (Figure 2B). Beside the substitution pattern on the BQCAd part, the length of the linker was varied in both series. In addition to using BQCA derived compounds for the allosteric binding moieties in these ligands, the *N*-piperidine benzimidazolone moiety of an allosteric agonist 1-(1′-(2-methylbenzyl)-1,4′-bipiperidin-4-yl)-1*H*-benzo[*d*]imidazol-2(3*H*)-one (TBPB) was also applied to connect it to **1** via linkers of different lengths (**5**, Figure 2C). The *N*-piperidine benzimidazolone moiety has been identified as an example for a key pharmacophoric structure of allosteric agonists (for review see ref 14).[14]

M_1 receptor activation and signaling behavior of the compounds were studied by monitoring dynamic mass redistribution (DMR) in live Chinese hamster ovary cells (CHO-*h*M_1) stably transfected with the human M_1 receptor.[42,43] A qualitative comparison at selected high concentrations in the absence and presence of specific blockers of G_i- and G_q-protein-mediated pathways revealed that the M_1 receptor effects of all hybrids were predominantly transmitted by G_q signaling. Concentration effect curves revealed partial agonism for M_1 receptor activation going along with submicromolar potency in case of hybrids **2**, **3**, and **4** but not **5**. The functional DMR data of all iperoxo/BQCAd hybrids (**2**,**3**) were analyzed by means of the operational model of agonism for dynamic ligands which had been introduced recently.[30] This model accounts for a switch of binding topography between an active pose and an inactive pose resulting in partial activation of the receptor population, i.e., partial agonism. The resulting "overall" coupling efficiency is quantified by the dynamic transduction coefficient τ_{dyn}.[30] In the present work, analysis of this functional data was extended by including binding data from separate experiments, applying a simultaneous global curve fitting procedure. This analytical one-step method allowed us to characterize conveniently the two selected iperoxo/BQCAd hybrids **2a** and **3a** regarding their respective functional affinities of the active (pK_{active}) and the inactive ($pK_{inactive}$) pose. This revealed a switch in favor of the ligand active binding pose from **2a** to **3a** by the elongation of the spacer length from C4 to C6. In addition, ε_{max}, i.e., the system-independent maximum intrinsic efficacy of the dynamic

dx.doi.org/10.1021/jm500860w | J. Med. Chem. XXXX, XXX, XXX−XXX

Scheme 2. Synthesis of M_1 Orthosteric Agonist Compound 1[a]

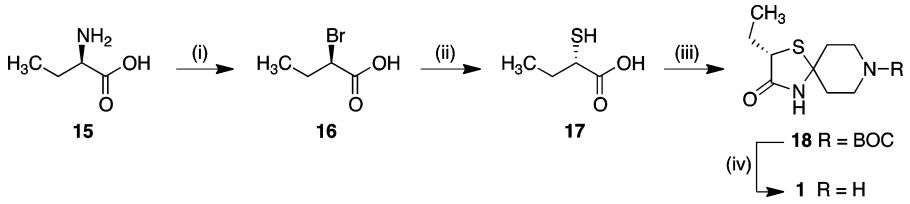

[a]Reagents and conditions: (i) $NaNO_2$ (1.2 equiv), KBr (3 equiv), HBr (47% soln), water, 0 °C to rt, 62%; (ii) (1) KOH (0.95 equiv), potassium ethyl xanthate (1.1 equiv), water, 50 °C, 2 h, (2) diethylenediamine dihydrochloride (2 equiv), KOH soln (4 equiv), 50 °C, 2 h, 61%; (iii) 1-Boc-4-piperidinone (0.7 equiv), $(NH_4)_2CO_3$ (1 equiv), benzene, reflux, 48 h, 63%; (iv) HCl (5 M in *i*PrOH), MeOH, rt, 24 h, 76%.

Scheme 3. Synthesis of Compound 1/BQCAd Hybrids[a]

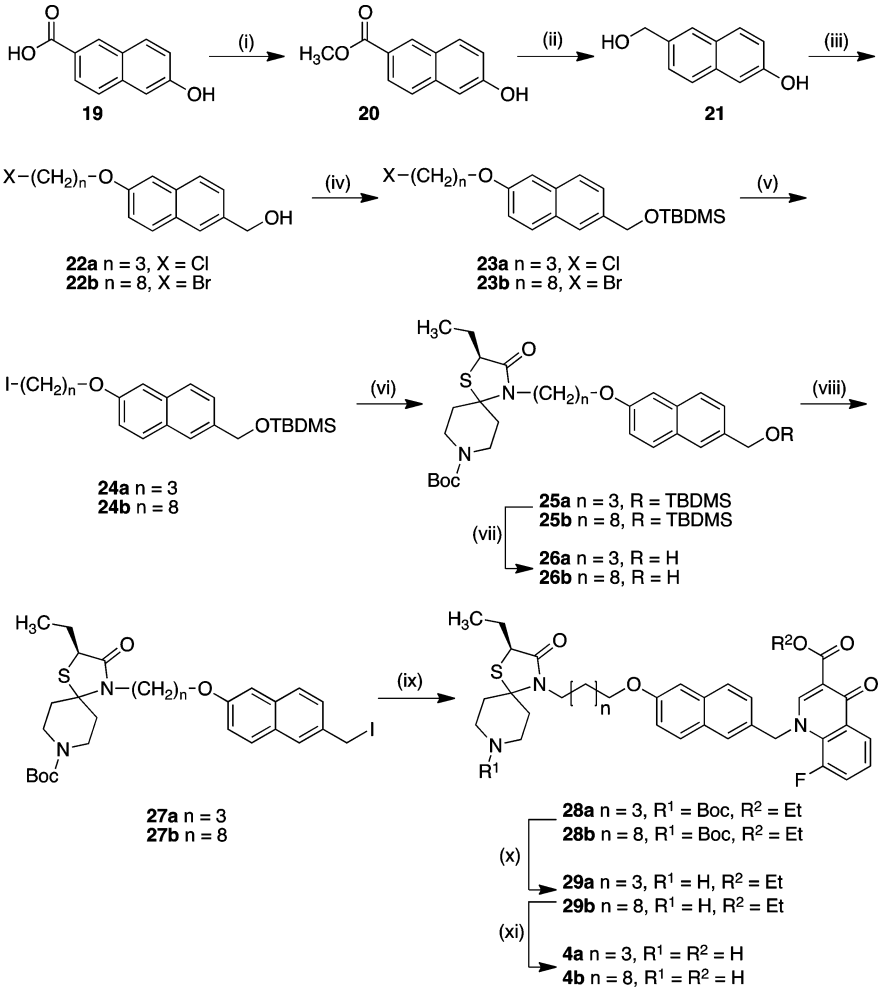

[a]Reagents and conditions: (i) conc H_2SO_4 (cat.), MeOH, reflux, 24 h; (ii) $LiAlH_4$ (2 equiv), dry THF, 0 °C to rt, 74% over two steps; (iii) NaOH (1.1 equiv), 1-chloro-3-iodopropane or 1,8-dibromooctane (1.1 equiv), CH_3CN/H_2O, 65–70 °C, 16 h, 72%; (iv) TBDMSCl (1.2 equiv), Et_3N (1.5 equiv), DMAP (cat.), CH_2Cl_2, rt, 16 h; (v) NaI (1.2 equiv), acetone, reflux, 16 h; (vi) NaH (60% in paraffin oil, 2 equiv), **18** (1.2 equiv), dry DMF, 0 °C to rt, 23% over two steps; (vii) $CH_3CO_2H/H_2O/THF$ 3:1:1, rt, 24 h, 78%; (viii) Ph_3P (1.6 equiv), imidazole (2.2 equiv), I_2 (1.5 equiv), CH_2Cl_2, 0 °C to rt, 68%; (ix) **9a** (1.1 equiv), Na_2CO_3 (2 equiv), 50 °C, 16 h, 42%; (x) HCl (5 M in *i*PrOH), MeOH, rt, 24 h, 50%; (xi) LiOH (2 equiv), $EtOH/H_2O$, rt, 24 h, 37%.

ligand in the active binding pose, has been estimated. The maximum intrinsic efficacy of **3a** was smaller compared to **2a** and, in view of the inverse pose ratios, thus explaining the resulting equal dynamic transduction coefficients τ_{dyn} of these hybrids. Thus, the rational design of bipharmacophoric partial agonists with a prevalent active binding pose was achieved for the first time in the case of muscarinic M_1 acetylcholine receptors.

RESULTS AND DISCUSSION

Chemistry. The quinolone skeleton (**9**) fitted with varying halogen substituents was built up using the Gould–Jacobs synthetic pathway making use of microwave assistance to facilitate conversion and provide high yields.[44] Benzylation of the quinolone nitrogen was achieved with benzyl chloride in the presence of K_2CO_3 and catalytic amounts of KI in DMF. The ester function (**10**) was amidated with the aminoalkyl

dx.doi.org/10.1021/jm500860w | J. Med. Chem. XXXX, XXX, XXX–XXX

Scheme 4. Synthesis of M_1 Allosteric Modulators Based on BQCA Naphthalene Derivatives[a]

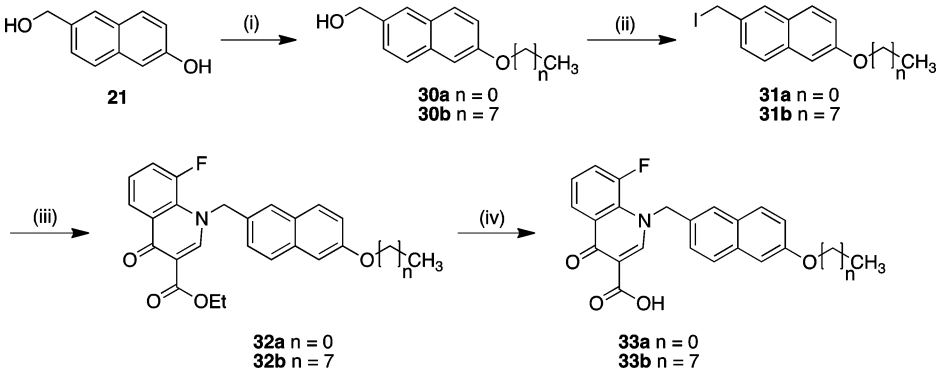

[a]Reagents and conditions: (i) NaOH (2 equiv), iodomethane or 1-bromooctane (1.2−1.5 equiv), CH_3CN/H_2O, 65−70 °C, 16 h, 98%; (ii) Ph_3P (1.6 equiv), imidazole (2.2 equiv), I_2 (1.5 equiv), CH_2Cl_2, 0 °C to rt, 42−50%; (iii) **9a**, Na_2CO_3 (2 equiv), DMF, 50 °C, 16 h, 46%; (iv) LiOH (2 equiv), $EtOH/H_2O$, rt, 24 h, 48%.

Scheme 5. Synthesis of M_1 TBPBd and the Corresponding 1/TBPBd Hybrids[a]

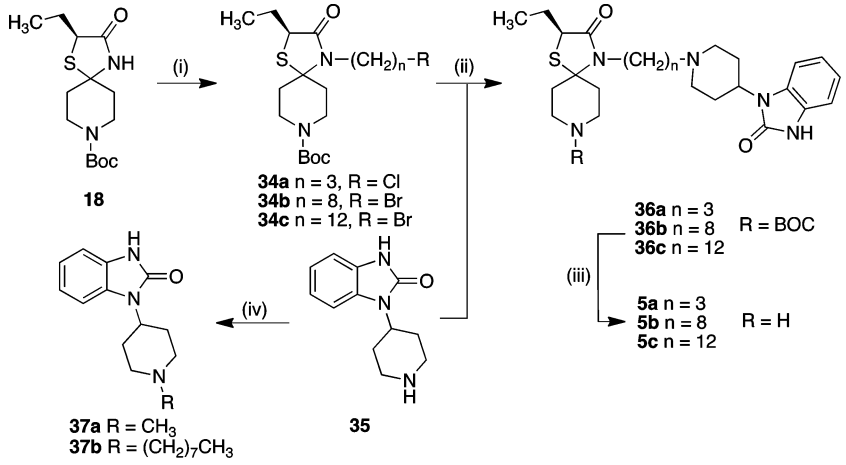

[a]Reagents and conditions: (i) NaH (60% in paraffin oil, 2.5 equiv), alkyl iodide (1.5 equiv), dry DMF, 0 °C to rt, 40%; (ii) Na_2CO_3 (2 equiv), DMF, 50 °C, 16 h, 45%; (iii) HCl (5 M in *i*PrOH), MeOH, rt, 24 h, 76%; (iv) dimethyl sulfate or 1-bromooctane (1 equiv), Na_2CO_3 (1.5 equiv), CH_3CN, reflux, 24 h, 45%.

alcohol of the corresponding spacer length (C4 and C6) and the hydroxyl function (**11**,**12**) substituted by a bromine atom using HBr/H_2SO_4. Finally, iperoxo, synthesized according to a method previously described,[45] was connected to the spacer (Scheme 1).

Because compounds **13** and **14** were subsequently applied as reference substances in the pharmacological assays, their inertness toward proteins were evaluated by incubation with glutathione under the same conditions as applied in the pharmacological assay system and proved no reaction as determined by LC-MS (data not shown).

The orthosteric agonist **1** was synthesized in a modified way as described in the literature:[39] 2-Bromobutyric acid (**16**) was synthesized from 2-aminobutyric acid (**15**) by diazotization and bromination in a Sandmeyer-like reaction. As described in the literature, stereochemical inversion took place using potassium ethyl xanthate. The configuration of the absolute stereocenter had been postulated based upon the mechanism of the reaction and the results reported in the literature.[39,46] Ring-closing was performed using ammonium carbonate and 1-Boc-4-piperidone.[39] After removing the BOC-group in acidic condition, compound **1** was obtained (Scheme 2).

Synthesis of bipharmacophoric ligands from compound **1** and BQCA-derived compounds started from the synthesis of the naphthalene-based linker intermediate (Scheme 3). 6-Hydroxy-2-naphthoic acid (**19**) was esterified (**20**) and reduced to the primary alcohol (**21**). Alkylation of this naphthol was achieved via Williamson ether synthesis with an α,ω-dihalogenoalkane followed by protection of the primary OH group with TBDMSCl. BOC protected compound **1** (**18**) could be alkylated at the lactam-*N* using alkyl iodide (**24**) obtained after Finkelstein reaction of the naphthol derivative (**23**). The TBDMS group was selectively removed in acetic acid/water/THF 3:1:1. Appel reaction was applied to replace the primary OH by an iodine atom.[47,48] The alkyl iodide **27** was in turn used to alkylate the fluoroquinolone carboxylate **9a**. BOC and ethyl ester groups were sequentially removed in acidic and basic conditions, respectively, to obtain the bipharmacophoric ligands (**4**, Scheme 3). The corresponding control compounds (**33a**,**b**), i.e., with the linker structures but without the orthosteric moiety, were also synthesized following the same synthetic strategy in order to evaluate the possible contribution of the linker structure to the receptor binding mode (Scheme 4).

dx.doi.org/10.1021/jm500860w | J. Med. Chem. XXXX, XXX, XXX−XXX

In addition to connecting BQCA-derived compounds to the M_1 agonist compound **1**, the *N*-piperidine benzimidazolone structure representing the core pharmacophore of allosteric agonist TBPB was also used to form a third series of bipharmacophoric hybrids (Scheme 5). Allosteric agonists by definition activate the receptor by binding to an allosteric site without concomitant binding of an orthosteric agonist being necessary for receptor activation.[14] First, alkylation of the thiazolidinone-*N* **18** was achieved by using NaH in dry DMF and an alkyl iodide, followed by reaction with *N*-piperidine benzimidazolone structure **35**, which was synthesized according to a literature protocol.[49] After BOC deprotection, the hybrids (**5a**−**c**) were obtained. The corresponding control compounds (**37a**,**b**), e.g., linker derived from the *N*-piperidine benzimidazolone structure, were synthesized by reacting the amine **35** with dimethyl sulfate or 1-bromooctane, respectively (Scheme 5).

DMR Measurements in *h*M_1-CHO Cells. Signaling of the compounds was evaluated by means of DMR measurements using live *h*M_1-CHO cells. The maximal system response was defined by the maximum response to saturating concentrations of the endogenous ligand acetylcholine (ACh). ACh and the M_2-superagonist iperoxo showed full agonism, whereas pilocarpine could be categorized clearly as a partial agonist (Figure 3C, Table 1). The functional affinities of the conventional agonists obtained according to the operational model[50] were in line with M_1 affinity measures published by others, i.e., $pK_{ACh} = 4.76 \pm 0.29$ with $pK_i = 4.90 \pm 0.11$[51] and $pK_{Pilo} = 5.57 \pm 0.11$ with $pK_{i,Pilo} = 5.1$.[52] Applying the operational model of agonism[50] to the DMR data of iperoxo, the transducer slope n was less than unity (F-test, $P < 0.05$). The functional affinity and the estimated operational efficacy of iperoxo at M_1 receptors amounted to $pK_{iperoxo} = 5.67 \pm 0.65$ and log $\tau_{iperoxo} = 2.99 \pm 0.65$, respectively (Table 1). The numerical estimate of $\tau_{iperoxo}$ indicates how far the concentration−effect curve of iperoxo in functional experiments is shifted to the left compared with its corresponding receptor binding curve. log $\tau_{iperoxo}$ was considerably though not significantly higher than log $\tau_{acetylcholine} = 1.64 \pm 0.28$ (Table 1; *t* test, $P > 0.05$). Thus, more-than-physiological agonism ("superagonism"), first demonstrated for iperoxo at the even-numbered, G_i-coupled M_2-subtype,[19] was not encountered at the odd-numbered, G_q-coupled M_1 subtype.

Potency values pEC_{50} of acetylcholine and iperoxo (Table 1) were far higher than their functional binding affinities p*K*. This finding reflected signal amplification by the assay system, also addressed as "receptor reserve". In the case of pilocarpine, however, pEC_{50} and p*K* were rather similar, and activation of the test system was far below the 100% level defined by the maximum effect of endogenous activator acetylcholine. Thus, pilocarpine behaved as a partial agonist.

*Structure−Signaling Relationships in Iperoxo/BQCAd-Type **2** and **3** Hybrids.* Concentration−effect curves for DMR of live *h*M_1-CHO cells as induced by the newly synthesized hybrid compounds **2** and **3** are shown in parts A and B of Figure 3, respectively. Data were analyzed by a four-parameter logistic equation (allowing a model-independent comparison of all compounds studied), and by means of the operational model of agonism for dynamic ligands,[30] the parameter values are summarized in Table 1. Like pilocarpine, the new test compounds **2** and **3** were partial agonists with E_{max} values of about 60%. Only compound **3b** reached a higher E_{max} of 80%. However, we are aware that a partial agonist in the

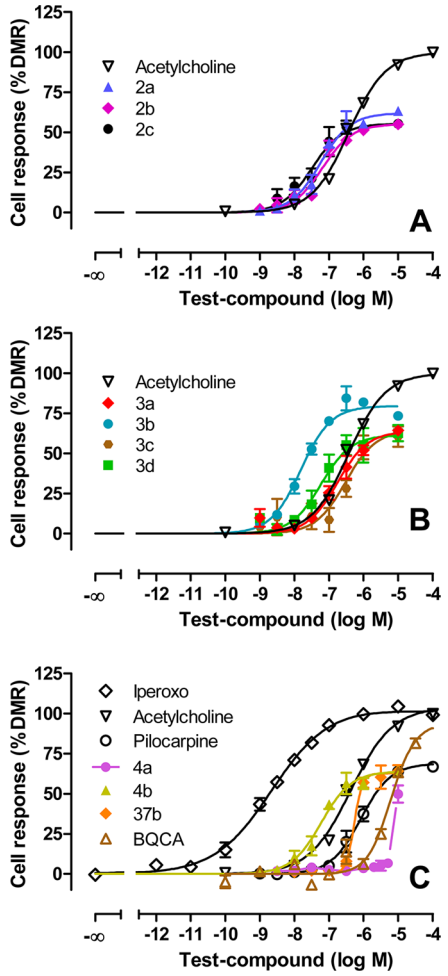

Figure 3. Iperoxo/BQCAd hybrids (**2a**−**c**, **3a**−**d**) and **1**/BQCAd (**4a**, **4b**) ligands act as partial M_1 agonists. Concentration−effect curves of positive DMR after 2400 s generated by the indicated orthosteric agonists and test compounds in live CHO-*h*M_1 cells. The data points in (A,B) and of **4b** in (C) were fitted to the operational model of agonism for dynamic ligands,[30] and the data of iperoxo, acetylcholine, and pilocarpine in (C) were fitted to the operational model of agonism.[50] The bottom and E_{max} values were constrained to 0 and 100%, respectively. Logistic curve fitting with variable slope was applied to the data points of **37b**. The DMR of solvent controls were set to 0% and the maximal positive DMR response in the presence of 100 μM acetylcholine to 100%. Data are means ± SEM from 3−12 independent experiments conducted in quadruplicate.

EPIC system applied in the current study may act as a full agonist in another system with higher signal amplification. In the classical operational model of agonism[50] and the operational model of agonism for dynamic ligands,[30] coupling efficiency is expressed by the parameters τ and τ_{dyn}, respectively. The dynamic efficacies τ_{dyn} of the test compounds ranged between log $\tau_{dyn,2b} = 0.09 \pm 0.03$ and log $\tau_{dyn,3b} = 0.59 \pm 0.04$ (Table 1). All iperoxo/BQCAd compounds (**2**, **3**) showed submaximum effects (Figure 3A,B), and their τ_{dyn} values were similar to τ of pilocarpine (Table 1). Thus, as intended by the rational design, the hybrid ligands **2**, **3** behaved as partial agonists. The difference in potencies (pEC_{50}) among members of the subgroup iperoxo/BQCAd hybrids **2a**−**c** amounted to 0.3 log units only. Obviously, the substitution pattern at the quinolone moiety had no relevant impact on hybrid potency (one-way ANOVA with Newman−Keuls

dx.doi.org/10.1021/jm500860w | J. Med. Chem. XXXX, XXX, XXX−XXX

Table 1. Measures of Potency and Efficacy of DMR Induced by Muscarinic Agonists and Hybrid Compounds in Live CHO-*h*M$_1$ Cells[a]

compd	*N*	R^1	R^2	R^3	pEC$_{50}$	%E_{max}	n_{op}	pK	log τ_{dyn}	n_{op}	*N*
acetylcholine					6.43 ± 0.04	100 ± 2	0.82 ± 0.07*	4.76 ± 0.29†	1.64 ± 0.28$^{\#}$	0.80 ± 0.07*	5
iperoxo					8.69 ± 0.06	102 ± 2	0.54 ± 0.04*	5.67 ± 0.65†	2.99 ± 0.65$^{\#}$	0.52 ± 0.03*	6
pilocarpine					6.08 ± 0.08	69 ± 3	1	5.57 ± 0.11†	0.35 ± 0.06$^{\#}$	1	3
2a	4	F	H	H	7.24 ± 0.09	62 ± 2	1	6.82 ± 0.10	0.21 ± 0.03	1	3
2b	4	H	Br	H	7.20 ± 0.10	55 ± 2	1	6.85 ± 0.11	0.09 ± 0.03	1	3
2c	4	H	Cl	F	7.49 ± 0.11	55 ± 2	1	7.14 ± 0.13	0.09 ± 0.03	1	5
3a	6	F	H	H	6.75 ± 0.09	64 ± 2	1	6.31 ± 0.11	0.25 ± 0.05	1	4
3b	6	H	Br	H	7.81 ± 0.13	80 ± 2	1	7.13 ± 0.11	0.59 ± 0.04	1	3
3c	6	H	Cl	F	6.52 ± 0.20	64 ± 6	1	6.07 ± 0.25	0.26 ± 0.11	1	4
3d	6	H	H	F	7.23 ± 0.09	61 ± 5	1	6.82 ± 0.27	0.20 ± 0.09	1	4
37b					6.27 ± 0.04	63 ± 2	3.64 ± 0.59*	nd‡	nd‡	nd‡	4
4a					nd‡	nd‡	nd‡	nd‡	nd‡	nd‡	8
4b					7.22 ± 0.09	64 ± 3	1	6.78 ± 0.11	0.25 ± 0.05	1	4
BQCA					5.08 ± 0.14	91 ± 14	1	4.26 ± 1.32	0.95 ± 1.13	1.33 ± 0.55	5

[a] pEC$_{50}$, concentration of the indicated compounds inducing a half-maximal DMR effect (−log EC$_{50}$ values); %E_{max}, maximum effect as a percentage of E_{ACh} (100 μM); *n*, slope factor obtained by curve fitting to data from individual experiments shown in Figure 3A,B using a four-parameter logistic equation; n_{op}, transducer slope applying the operational model of agonism;[30,50] *, significantly different from unity (F-test, $P < 0.05$); log τ_{dyn}, operational efficacy; pK = −log K_D (see Experimental Section, Data Analysis, eq 1) measures of functional affinities were derived from DMR data according to the operational model of agonism for dynamic ligands;[30] † value is pK = − log K; # value is log τ, according to the operational model of agonism;[50] nd, not determined; ‡, fit was ambiguous. Data are means ± SEM of *N* independent experiments conducted as quadruplicate determinations.

multiple comparison test, $P > 0.05$). In contrast, among the iperoxo/BQCAd hybrids **3a−d** containing the elongated C6-linker, differences in pEC$_{50}$ values of 1.3 log units were observed, indicating that the substitution pattern affected ligand potency. Furthermore, potencies of hybrids with a C4- (**2a−c**) versus a C6-spacer (**3a−d**) were lower or higher depending on the pattern of substitution in the benzyl quinolone moiety. The difference in pEC$_{50}$ reached statistical significance *within* the C6 series with **3a** vs **3b** and **3d**, **3b** vs **3c** and **3d**, **3c** vs **3d** and *between* the C4 and C6 series with **2a** vs **3a**, **3b**, and **3c** as well as **2b** vs **3a**, **3b**, and **3c** and **2c** vs **3a** and **3c**. With respect to the differences in E_{max}, statistical significance was observed *within* the C6 series with **3b** vs **3a**, **3c**, and **3d**, and *between* the C4 and C6 series with **2a** vs **3b**, **2b** vs **3b**, and **2c** vs **3b** (one-way ANOVA with Newman−Keuls multiple comparison test, $P < 0.05$). It is worth mentioning that test compound-induced DMR was blocked by the muscarinic antagonist atropine, 10 μM, and did not occur in "empty" live CHO K1 cells lacking the M$_1$ receptor, thus demonstrating that effects were mediated by the M$_1$ receptor (data not shown). Taken together, changing the length of the hybrid spacer in conjunction with the pattern of substitution allowed showing that dynamic ligand binding tunes the efficacy of iperoxo/BQCAd-type **2** and **3** hybrids in *h*M$_1$-CHO cells.

Structure−Signaling Relationships in 1/BQCAd-Type Hybrids 4. Compared to DMR induced by ACh (see above), **1**, which had been claimed to be an M$_1$ agonist,[39] only showed a weak maximum effect of 12 ± 3% at a concentration of 10 μM (Figure 4C, Supporting Information, Figure 1). Nevertheless, we used **1** as an orthosteric moiety in our hybrid molecules. As can be seen in Figure 4C carried out as a comparison of the effects *E* at a single concentration (the respective highest dissolvable compound concentration with less than 1.3% DMSO in the assay, cf. Materials and Methods for further details) linkage of **1** with the inefficacious allosteric moieties **33a** (0.3 μM: E = 1 ± 1%) and **33b** (1 μM: E = 1 ± 1%) yielded the **1**/BQCAd hybrids **4a** (10 μM: E = 55 ± 11%) and **4b** (10 μM: E = 61 ± 9%). The concentration−effect relationship of **4b** (Figure 3C, Table 1) showed "normal" partial agonism with a submaximum effect and a τ_{dyn} value similar to τ of pilocarpine (Figure 3C, Table 1). Thus, as intended by the rational design, the hybrid ligand **4b** behaved as a partial agonist. The **1**/BQCAd hybrid **4a** at a rather high concentration of 10 μM induced a brisk M$_1$ receptor mediated DMR response (Figure 3C) which could be abolished by 10 μM atropine (data not shown). As illustrated in Figure 3C, **4a** had a steep concentration−effect relationship, suggesting a peculiar, unknown mechanism of agonism and could not be fitted unambiguously by applying the operational model of agonism (Table 1). Compound **4a** had a very low potency with an effect only at 10 μM (higher concentrations were not applicable due to poor solubility).

Structure−Signaling Relationships in 1/TBPDd-Type 5 Hybrids. The **1**/TBPBd-type hybrids **5a**, **5b**, and **5c** lacked any DMR effect; they were inactive (Supporting Information, Figure 1). Interestingly, the TBPBd **37b** triggered a very steep response, which, however, leveled off at about 50%, but three data points defined an upper plateau, thus allowing derivation of a potency, a maximum effect, and a slope factor. (Figure 3C, Table 1). The steep concentration−effect relationship of **37b** suggested a peculiar, unkown mechanism of agonism and could not be fitted unambiguously applying the operational model of agonism (Table 1). The effect of **37b** was likely to occur allosterically because **37b** retarded the dissociation of the orthosteric radioligand [^{3}H]NMS from M$_1$ receptors in live CHO-*h*M$_1$ cells (Supporting Information, Figure 2). The half-maximal inhibitory action of **37b** with regard to allosteric inhibition of [^{3}H]NMS dissociation, pEC$_{0.5,diss,37b}$ = 5.94 ± 0.08, N = 3, occurred in the micromolar concentration range. The maximum percent reduction of k_{-1} by **37b** was observed at 36 ± 3% (Supporting Information, Figure 2). The latter was equivalent to a 3-fold retardation of [^{3}H]NMS dissociation

dx.doi.org/10.1021/jm500860w | J. Med. Chem. XXXX, XXX, XXX−XXX

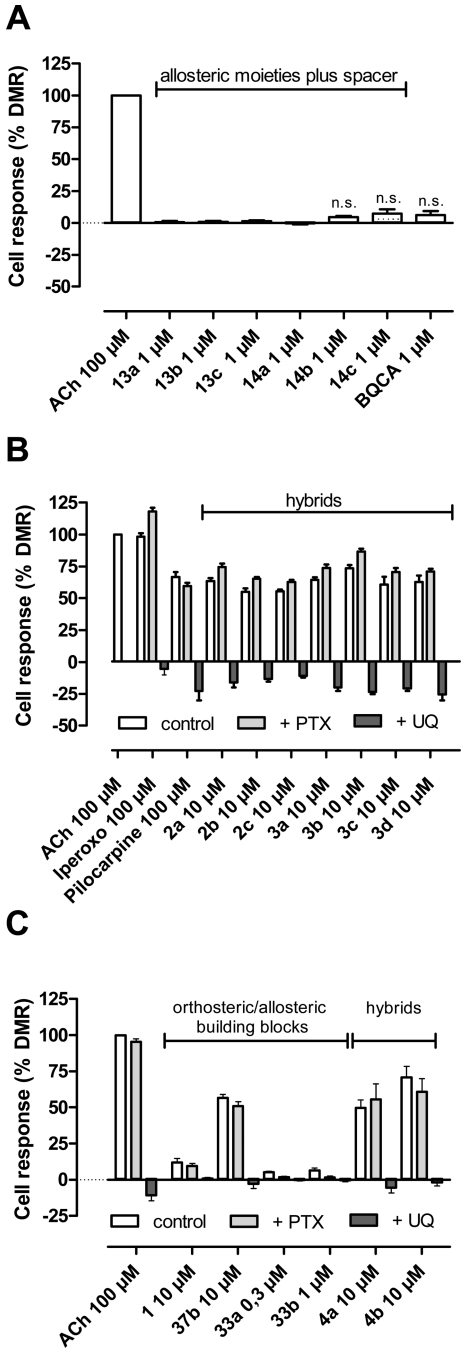

Figure 4. M_1 agonist efficacy does not depend on (A) the allosteric moieties (**13**, **14**) in iperoxo/BQCAd-prototype hybrids (**2**, **3**), whereas it depends (C) on "hybridization" in **1**/BQCAd hybrids (**4**) and is (B,C) mainly mediated via G_q proteins. DMR in live CHO-hM_1 cells generated after 2400 s by the indicated orthosteric agonists and test compounds under (A) control conditions and, additionally (B,C), after pretreatment with PTX (100 ng/mL, overnight) for inhibition of G_i- or UQ (1 μM, 1.5 h prior to the DMR measurement) for inhibition of G_q coupling, respectively. The DMR were solvent-corrected and expressed as percent of the maximal positive DMR response in the presence of 100 μM acetylcholine. n.s., not significant, one sample *t*-test, $P > 0.05$. Data are means ± SEM from 3−12 independent experiments conducted in quadruplicate.

relative to control conditions ($t_{1/2,diss}$ = 8.9 ± 0.3 min, N = 21) by **37b**. This behavior is undoubtedly indicative of an allosteric action because the orthosteric M_1 receptor site is occupied by the radioligand.[53] In conclusion, the agonist action of **37b** involves the allosteric site in hM_1 receptors. Taken together, the series of **1**-derived bipharmacophoric compounds revealed complexities which are currently not fully understood on the molecular level and will be investigated further.

*Ineffectivity of Iperoxo/BQCAd-Type **2**, **3** Hybrids Lacking Their Iperoxo Moiety.* The partial- to full-agonistic action that had been reported for the parent compound BQCA[34−37] was also found in the current study (Figure 3C, Table 1). To rule out the possibility that the respective allosteric building blocks, i.e., bromoalkylamides of the benzyl quinolones, were responsible for receptor activation by the iperoxo/BQCAd hybrids (**2**, **3**), we checked whether they had a DMR effect on their own. The compounds **13a**, **13b**, **13c**, **14a**, **14b**, and **14c** and the prototypal BQCA at a concentration of 1 μM did not produce a DMR signal (Figure 4A, one sample *t* test, $P > 0.05$). **13a** and **14a**, the allosteric building blocks of the hybrids **2a** and **3a**, respectively, which were studied in greater detail (see below), both at 1 μM reached the maximum level of allosteric inhibition of [^{3}H]NMS binding (Figure 5B,D). This bottom level is above zero, suggesting allosteric ternary complex formation including receptor, radioligand, and test compound. A closer look at the concentration-dependent effects of **13b,c** and **14b,c** included in Figure 4A revealed slightly smaller binding affinities $pK_{inactive}$ compared to **13a** and **14a** but a similar submaximum [^{3}H]NMS displacement at high concentrations of 3 and 10 μM, respectively (Supporting Information, Figure 3A,B). This reflects moderately negative cooperativity between **13a,b,c** and **14a,b,c** and the orthosteric [^{3}H]NMS with cooperativity factors ranging between log α'_{14a} = −0.82 ± 0.04 and log α'_{14c} = −1.35 ± 0.57 (**13a**, **14a**, Table 2, and **13b,c**, **14b,c**, Supporting Information, Figure 3, respectively). Since it might be argued that **13a,b,c** and **14a,b,c** nevertheless may bear the allosteric agonistic potential of the prototypal BQCA but at higher concentrations, we aimed at increasing the concentrations studied in the EPIC system. However, **13a,b,c** and **14a,b,c** had to be dissolved in DMSO, and the DMSO content of their dilutions in buffer prevented studying higher concentrations than 1 μM in the EPIC system due to a solvent effect of DMSO (for further details see Materials and Methods). Because M_1 receptor-mediated IP1 accumulation in CHO-hM_1 cells is less sensitive to DMSO compared to the signal generated in the EPIC system, it allowed us to increase the concentration of **13a,b,c** and **14a,b,c** up to a concentration of 10 μM. In the IP1 assay, iperoxo, acetylcholine, **2a**, and **3a**, but not BQCA showed somewhat higher potencies but very similar efficacies (Supporting Information, Figure 4) compared to the respective parameters obtained in the EPIC sytem (Table 1). Thus, the potency and efficacy profiles of these ligands in both assay systems were similar. BQCA was a full agonist in the EPIC system and a partial agonist in the IP-1 assay. In Supporting Information, Figure 5, it can be seen that in the IP1-assay, BQCA (10 μM) was significantly active but **13a,b,c** and **14a,b,c** remained inactive. Taken together, the agonistic action that had been reported for the parent compound BQCA[34−37] was not shared by our BQCA derivatives. Most importantly in the present context, the absence of an agonist action of **13a,b,c** and **14a,b,c** allowed us to apply the operational model of agonism for dynamic ligands[30] in order to check whether efficacy is related to binding pose. This was studied exemplarily with the two selected iperoxo/BQCAd hybrids **2a** and **3a** (see below).

dx.doi.org/10.1021/jm500860w | J. Med. Chem. XXXX, XXX, XXX−XXX

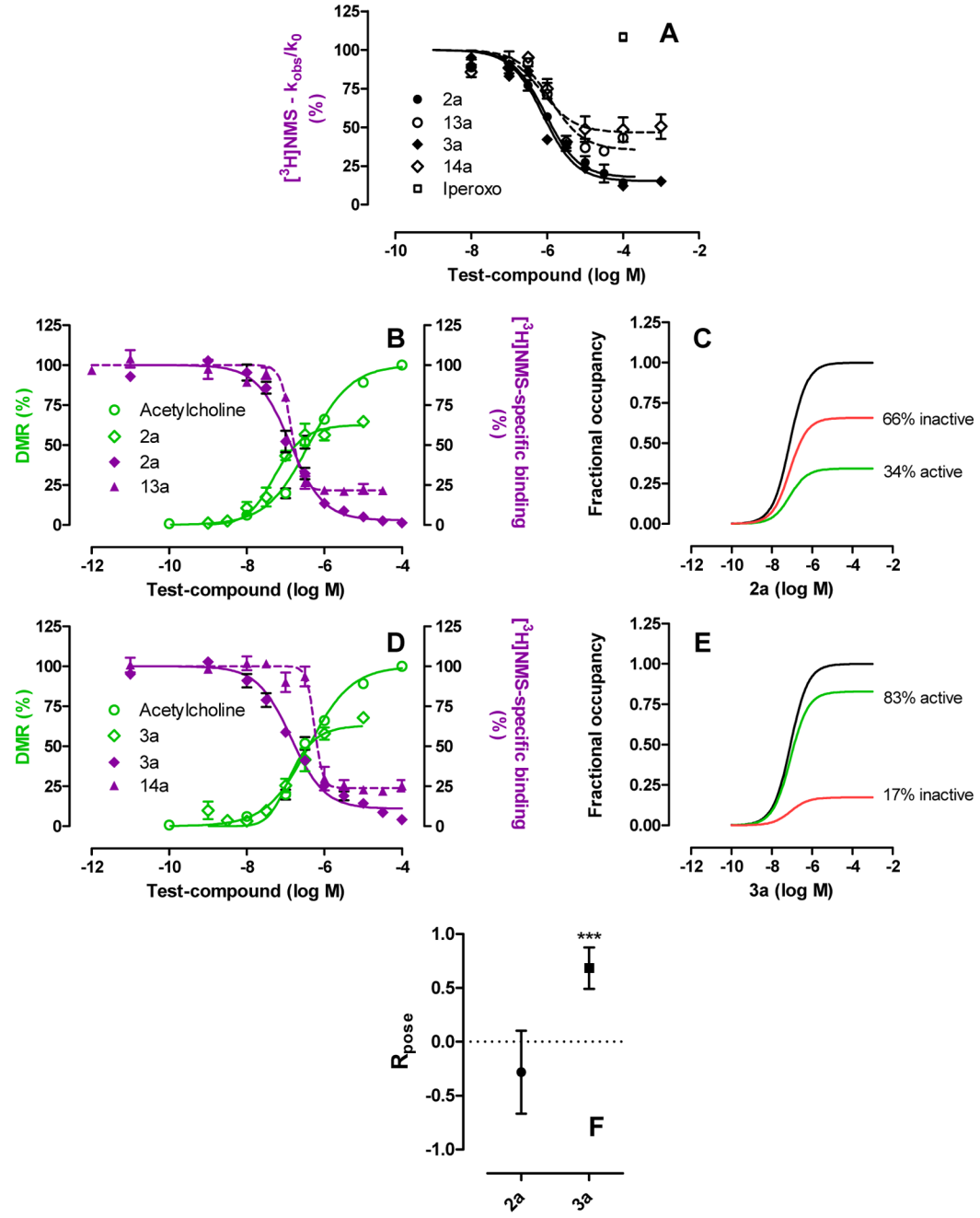

Figure 5. (A) Allosteric effects of the hybrids (**2a**, **3a**) and their corresponding allosteric moieties (**13a**, **14a**) as reflected by the inhibition of [^{3}H]NMS dissociation from M_1 receptors in live CHO-*h*M_1 cells. The allosteric effect is expressed as the ratio of the rate of [^{3}H]NMS dissociation in the presence of compound (k_{obs}) relative to the rate of dissociation of [^{3}H]NMS in the absence of test compound (k_0), expressed in percent. Iperoxo at a high concentration did not retard [^{3}H]NMS dissociation (B–F). Switch of the fractional active binding pose of the iperoxo/BQCAd-hybrid **2a** and **3a** derived from global data analysis by the operational model of agonism for dynamic ligands. (B,D) Effect of increasing concentrations of ACh and of the respective hybrid in percent DMR (left ordinate, data taken from Figure 3A) and of the respective hybrid and its allosteric moiety on specific percent equilibrium binding of [^{3}H]NMS (right ordinate) in live CHO-*h*M_1 cells. (C,E) Concentration-dependent fractional receptor occupancy of the receptor active and inactive binding poses of **2a** and **3a**. Global curve fitting to sets of four curves included in (B,D) eq 3, for details, cf. text and Experimental Section. Data in A–E represent mean ± SEM from 3–4 independent experiments, conducted in quadruplicate. (F) Note the significant switch of the fractional receptor occupancy to the active hybrid binding pose (means ± 95% CI) upon spacer elongation between **2a** and **3a** (*t*-test, $P < 0.001$, see text for discussion).

*Effects of Iperoxo/BQCAd-Type **2**, **3** and **1**/BQCAd-Type **4** Hybrids Are Predominantely Mediated by G_q Proteins.* In the presence of the G_q protein inhibitor UBO-QIC (alternatively called UQ, FR900359, structure cf. Supporting Information) (Figure 4B,C), no positive DMR signal could be detected for any of the compounds; merely a tiny negative DMR signal remained which may represent a G_s-coupling component. Thus, all active hybrid molecules behaved as partial agonists characterized by a $\%E_{max}$ value between 55 and 80% (Figure 3, Table 1) and activated predominantly the G_q-signaling pathway (Figure 4B,C). In the presence of the G_i protein inhibitor pertussis toxin (PTX), M_1 receptor-mediated signaling of

dx.doi.org/10.1021/jm500860w | J. Med. Chem. XXXX, XXX, XXX–XXX

Table 2. Measures Obtained by Global Simultaneous Analysis of Hybrid Functional and Binding Data with the Operational Model of Agonism for Dynamic Ligands in Live CHO-*h*M_1 Cells[a]

compd	N	pK_{active}	$pK_{inactive}$	log τ_{dyn}	R_{pose}	log ε_{max}*
2a	4	6.64 ± 0.15	6.92 ± 0.04	0.15 ± 0.02	−0.28 ± 0.19	0.61 ± 0.13
3a	6	6.98 ± 0.06	6.30 ± 0.05	0.08 ± 0.01	0.68 ± 0.09	0.17 ± 0.02

[a] N, spacer length between the orthosteric and the allosteric moiety; pK_{active}, $pK_{inactive}$, (−log) equilibrium dissociation constants of the dynamic ligand for the active pose and for the inactive receptor binding pose, respectively. pK_{active} equals pK_A; note that $pK_{inactive}$ equals the equilibrium dissociation constant pK_B of the respective allosteric moiety (**13a**, **14a**) at the free receptor; log τ_{dyn}, log dynamic transduction coefficient of the ligand; R_{pose}, −log $K_{active}/K_{inactive}$, i.e., the −log ratio of the equilibrium dissociation constants of the active and the inactive receptor binding pose; ε_{max}*, system-independent maximum intrinsic efficacy of the dynamic ligand at 100% occupancy in the active pose in the absence of receptor reserve. Data are parameter estimates ± SEM of global fits to CECs (1−4) (cf. Experimental Section) characterizing the respective hybrid each carried out as 3−4 independent experiments conducted as quadruplicate determinations. log ε_{max}* was determined in separate analyses (involving eq 7, cf. Discussion, not included in Figure 5) in which log τ_{dyn} was replaced by ε_{max} and R_T/K_E (involving eq 6, cf. Experimental Section). For **2a** and **3a**, global curve fitting with R_T/K_E = 1 = constant yielded ε_{max}*. For further details, see Results, Discussion, and Experimental sections.

receptor saturating concentrations of ACh, iperoxo, and pilocarpine (100 μM, Figure 4B) as well as high concentrations of the hybrids (10 μM, Figure 4B,C) was hardly affected.

Interestingly, the DMR signal of the allosteric moiety **37b** was likewise mainly G_q-mediated (Figure 4C); this may suggest that this signaling pathway can also be activated through the allosteric binding area of M_1 receptors.

*Fractions of Iperoxo/BQCAd-Type **2**, **3** Hybrid Binding Poses Estimated by Means of the Operational Model of Agonism for Dynamic Ligands.* To quantify the percentage of active receptor pose of selected iperoxo/BQCAd hybrids, we additionally performed binding experiments with both hybrids and their allosteric moieties (**13a** and **14a**, respectively) in live CHO-*h*M_1 cells using [^{3}H]NMS as the orthosteric radioactive probe. We chose the pair **2a** and **3a** that differ structurally in spacer length and pharmacologically solely in potency (i.e., pEC_{50}) (one-way ANOVA with Newman−Keuls multiple comparison test, $P < 0.05$, cf. Table 1) but not with respect to E_{max} and log τ_{dyn}. Preconditions for the applicability of the operational model of agonism for dynamic ligands[30] to hybrid data are an agonistic effect of its orthosteric but not of its allosteric moiety. Furthermore, to be capable of adopting a dualsteric receptor binding pose, the hybrid and its corresponding allosteric moiety should be able to interact allosterically with orthosterically blocked receptors; on the other hand, iperoxo should not. To check for an interaction with the allosteric site in [^{3}H]NMS-occupied M_1-receptors, we measured the effect of the hybrids **2a** and **3a**, of their allosteric moieties **13a** and **14a**, and of iperoxo on the apparent rate constant k_{-1} of radioligand dissociation (Figure 5A). The half-maximal inhibitory concentration with regard to the rate constant k_{-1} of [^{3}H]NMS dissociation ($pEC_{0.5,diss}$) of both the hybrids **2a** ($pEC_{0.5,diss}$ = 6.04 ± 0.08, N = 3) and **3a** ($pEC_{0.5,diss}$ = 6.10 ± 0.07, N = 3) and their allosteric moieties **13a** ($pEC_{0.5,diss}$ = 5.90 ± 0.13, N = 3) and **14a** ($pEC_{0.5,diss}$ = 6.15 ± 0.21, N = 3) occurred at micromolar concentrations. The corresponding maximum percent reduction of k_{-1} by the compounds were observed at **2a** = 18 ± 3, **3a** = 15 ± 3, **13a** = 35 ± 4, and **14a** = 47 ± 5 (cf. Figure 5A). The latter were equivalent to a 7- and 2-fold retardation, by the hybrids or allosteric moieties, respectively, of [^{3}H]NMS dissociation under control conditions. The curves showed slopes not different from unity (F-test, $P > 0.05$). No compound blocked [^{3}H]NMS dissociation completely. Yet, a complete block of [^{3}H]NMS dissociation is not a prerequisite to identify an allosteric interaction of a compound with a receptor site because an allosteric ligand may reduce but not fully inhibit the probability of orthosteric radioligand dissociation. Taken together, these hybrids and their allosteric moieties but not iperoxo bound to the allosteric site of M_1 receptors in live CHO-*h*M_1 cells. Because the allosteric moieties **13a** and **14a** on their own did not show an agonistic action (Figure 4A and Supporting Information, Figure 5), whereas the orthosteric iperoxo did (Figure 3B and Supporting Information, Figure 4), we concluded a dualsteric M_1 receptor interaction of **2a** and **3a**. Finally, we looked for a potential PAM effect of **2a**, **3a**, **13a**, and **14a** on acetylcholine binding to *h*M_1 receptors. From the inspection of the insets of Supporting Information, Figure 6A−D, it can be seen that neither of them induced a left shift of the inhibitory effect of acetylcholine on specific [^{3}H]NMS equilibrium binding to *h*M_1-receptors; instead, at compound concentrations indicating their strong negative cooperativity with NMS by the reduction of the upper plateau of the respective [^{3}H]NMS control curves (Supporting Information Figure 6A−D), **2a**, **3a**, **13a**, and **14a** significantly reduced the $pIC_{50,acetylcholine}$, suggesting a negative cooperativity with acetylcholine (F-test, $P < 0.05$). Therefore, we checked for dynamic ligand binding by applying a corresponding model reported recently.[30] Sets of four curves as shown in Figure 5B,D (i.e., ACh-induced DMR, hybrid-induced DMR, [^{3}H]NMS equilibrium displacement by the hybrid and by its respective allosteric moieties) were subjected to the "first" global nonlinear regression analysis including the operational model of agonism for dynamic ligands (for fitting details see Experimental Section). This yielded numerical estimates for the parameters pK_{active} and $pK_{inactive}$ of hybrid binding in the active and inactive binding pose, respectively and, moreover, for τ_{dyn}, n_{OP} (transducer slope of eq 1), α'_{hybr}, α'_{frag}, and n_{frag} (slope of eq 5) The novel global approach introduced here *joins* functional *and* binding data, allowing pK_{active} to be estimated from function *and* binding simultaneously and does neither predefine $pK_{inactive}$ nor the cooperativity α' of the hybrid with [^{3}H]NMS by that of its allosteric moiety (for further details cf. Materials and Methods, data analysis, and Supporting Information, Figure 7). The rationale of this approach was that global fitting with shared affinities pK_{active} and $pK_{inactive}$ but with individual cooperativities log α'_{hybr} and log α'_{frag} of the dynamic ligand and its allosteric fragment with [^{3}H]NMS, respectively, would come closer to reality than fixing $pK_{inactive}$ and log α'_{hybr} to those values obtained in [^{3}H]NMS displacement experiments with the allosteric fragment. Curve fitting revealed the curve slopes n_{frag} of **13a** and **14a** (global approach, Figure 5B,D, Supporting Information, Table 1) and of **13b** and **14b** but not of **13c** and **14c** (cf. single curve analyses, Supporting Information, Figure 3) to be significantly

dx.doi.org/10.1021/jm500860w | J. Med. Chem. XXXX, XXX, XXX−XXX

larger than unity (F-test, $P < 0.05$). Currently, we have no explanation for the high steepness.

The estimates of pK_{active} and $pK_{inactive}$ (Table 2) served to calculate the fractional receptor occupancy in the dualsteric and the allosteric pose, respectively (Figure 5C,E) and to derive corresponding R_{pose} values (for details see Experimental Section). A complete compilation of the parameters, their numerical estimates and treatment in the global fitting procedure is given in Supporting Information, Table 1. It became obvious that increasing the spacer length from C4 in **2a** to C6 in **3a** reduced binding in the inactive pose and, vice versa, augments binding in the active receptor pose (cf. Figure 5C,E). The difference in R_{pose} values of **2a** and **3a** was statistically significant (*t*-test, $P < 0.05$, Figure 5F, Table 2).

To show that the resulting R_{pose} values are robust, we analyzed the dynamic ligands **2a** and **3a** with a "second" version of the global fit where α'_{hybr} and α'_{frag} were treated as shared variables and n_{frag} was constrained to unity (Supporting Information, Table 2 and Figure 7C,E). Most importantly, the significant switch in R_{pose} between compounds **2a** and **3a** was maintained (*t*-test, $P < 0.05$), although the resulting values were slightly different (Supporting Information, Figure 7F).

*The Intrinsic Receptor Activity of **2a** and **3a** Bound in the Active Pose Plus the Fraction of Active Pose Govern Their Maximum Effect.* In view of the difference in R_{pose} values between **2a** and **3a** (Table 2), i.e., the differing fractions of active pose, the question arose why both compounds **2a** and **3a** shared the same maximum effect (cf. Table 1: $\%E_{max}$ 62 ± 2 and 64 ± 2, respectively, corresponding to operational efficacies τ_{dyn} 0.21 ± 0.03 and 0.25 ± 0.05). In this context, it is necessary to note that signaling of the bitopic compounds does not only depend on the probability of binding in the signaling-competent pose but also on the intrinsic efficacy generated by a ligand in the active pose.[54]

Therefore, the parameter τ_{dyn} was resolved into the system-independent maximum intrinsic efficacy of the dynamic ligand ε_{max} (corresponding to the activity of the individual ligand/receptor complex with agonist bound in the active pose) and R_t/K_E as a measure of the receptor reserve (for further details, see Experimental Section). Because the cells and the conditions applied in the experiments with hybrids **2a** and **3a** were identical, we constrained for a comparison of their ε_{max} values the parameter R_t/K_E to one same value in the respective global fits. ε_{max} obtained with $R_t/K_E = 1$ = constant equals τ_{max} in the absence of a receptor reserve (i.e., $R_t/K_E = 1$; cf. Experimental Section) and was termed ε_{max}*. These ε_{max}* values allowed a comparison of **2a** and **3a** with regard to the system-independent maximum intrinsic efficacy of the dynamic ligand at 100% occupancy of receptors in the active pose (Table 2).

Because the difference in ε_{max}* is significant (*t* test, $P < 0.05$), the findings indicated that compound **2a** surpasses **3a** with respect to intrinsic efficacy in the signaling competent dualsteric binding pose. This explained why the overall dynamic transduction coefficient τ_{dyn} for DMR did not differ between **2a** and **3a** (Table 1). Furthermore, analysis of ligand efficacy beyond the E_{max} of the measured response, i.e., the consideration of the agonist−receptor complex related efficacy ε_{max}* in combination with the probability of ligand receptor binding in the signaling-competent pose offers an additional way to differentiate ligand efficacy in a graded fashion.

To summarize, the feasibility of dynamic ligand binding to achieve designed partial agonism at muscarinic M_1 receptors is shown for the first time. Future studies will address the muscarinic receptor subtype selectivity of effects shown by the BQCAd-hybrid compounds. In M_1 receptors, employing a bitopic orthosteric/allosteric design concept the appropriate choice of building blocks allows to set signaling to the desired level of efficacy.

CONCLUSIONS

Three series of hybrid compounds have been synthesized and studied, and the findings reported here clearly demonstrate that bipharmacophoric iperoxo/BQCAd (**2**, **3**) and **1**/BQCAd (**4**) but not **1**/TBPBd (**5**) hybrid ligands are able to act as partial hM_1 receptor agonists. The effects of the former have pilocarpine-like efficacy and functional affinity and are mediated mainly through the physiologically relevant G_q-signaling pathway. We conclude that the hybrid approach to generate partial M_1 receptor agonists is sound as the findings suggested that hybrid potency and efficacy depended on the spacer length between the orthosteric and allosteric moieties in conjunction with the pattern of substitution in the allosteric moieties. In addition, increasing the spacer length between the orthosteric and allosteric moieties of selected hybrids in the iperoxo/BQCAd series (**2**, **3**) enhanced the fractional receptor occupancy in the receptor active binding pose and lowered the system-independent maximum intrinsic efficacy of the dynamic ligand ε_{max} in the active binding pose while preserving partial agonist activity. Thus, M_1 partial agonism can be designed by bipharmacophoric hybrid formation and fine-tuned with respect to the fraction of the M_1 receptor active hybrid binding pose and its efficacy. The combination of bipharmacophoric partial agonist design and active receptor binding pose tuning represents an important new step of current GPCR drug design and may, in muscarinic M_1 receptors, become therapeutically exploitable, e.g., in states of AD.

EXPERIMENTAL SECTION

Chemistry. *General Methods for Synthesis.* Melting points are uncorrected and were measured in open capillary tubes, using a Barnstead Electrothermal IA9100 melting point apparatus. ^1H and ^{13}C NMR spectral data were obtained from a Bruker Advance spectrometer (300 and 75 MHz, respectively). TLC was performed on silica gel on aluminum foils with fluorescent indicator 254 nm (Fluka) or aluminum oxide on TLC-PET foils with fluorescent indicator 254 nm (Fluka). For detection iodine vapor or UV light (254 nm) were used. ESI-MS samples were analyzed using electrospray ionization ion-trap mass spectrometry in nanospray mode using a Thermo Finnigan LCQ Deca. For column chromatography, silica gel 60, 230−400 mesh (Merck) was used.

The purities of the final new compounds (**2a−c**, **3a−d**) were determined using capillary electrophoresis and were found to be ≥95%. The CE analyses were performed on a Beckman Coulter P/ACE System MDQ (Fullerton, CA, USA), equipped with an UV-detector measuring at 210 nm, using a fused silica capillary (effective length 40 cm, total length 50.2 cm, diameter 50 μm) and as a running buffer 50 mM aqueous sodium borate, pH 10.5. Prior to use, aqueous solutions were filtered through a 0.22 μm pore-size CME (cellulose mix ester) filter (Carl Roth GmbH, Karlsruhe, Germany). The aqueous buffer was prepared using ultrapure Milli-Q water (Millipore, Milford, MA, USA). Purity of all other target compounds (**4a**,**b**, **5a−c**) was evaluated either by elemental analysis or by high-resolution mass following HPLC system (confirming purity ≥95%). Analytical HPLC using a VWR Hitachi L-2130 pump coupled to VWR Hitachi column oven L-2350 and L-2455 diode array detector. The solvents were as follows: (A) water + 0.05% trifluoroacetic acid and (B) acetonitrile + 0.05% trifluoroacetic acid; flow, 0.4 mL/min. Column Hibra 125-4 Purospher STAR RP-18e (3 μm) at 20 °C, detecting at 249 nm;

dx.doi.org/10.1021/jm500860w | J. Med. Chem. XXXX, XXX, XXX−XXX

solvent A from 90% to 10% for 30 min, then 10% for 15 min, from 10% to 90% for 10 min, 90% for 5 min.

*(S)-1-((6-(3-(2-Ethyl-3-oxo-1-thia-4,8-diazaspiro[4.5]decan-4-yl)-propoxy)naphthalen-2-yl)methyl)-8-fluoro-4-oxo-1,4-dihydroquinoline-3-carboxylic Acid (**4a**).* To the solution of **29a** (40 mg, 0.06 mmol) in tetrahydrofuran (10 mL) and water (5 mL) was added lithium hydroxide (5 mg). The resulting solution was stirred at room temperature for 24 h. The mixture was frozen under liquid nitrogen and concentrated under high vacuum to yield the target compound **4a** as yellow grease (30 mg, 60%).

*General Procedure for the Synthesis of the Diethyl Anilinomethylenemalonates **8a–d**.* According to the method described by Leyva et al.[44] and de la Cruz et al.,[55] 30 mmol of the corresponding aniline derivative and 36 mmol of diethyl ethoxymethylenemalonate were suspended in toluene and refluxed for 6–24 h. Then, the solvent was evaporated in vacuo, and 200 mL of pentane was added to the residue. The solution was kept at 4 °C for several hours. The crystals were collected, washed with pentane, and dried in vacuo.

*General Procedure for the Synthesis of Compounds **9a–d**.* First, 40 mmol of the diethyl anilinomethylenemalonates **8a–d**, respectively, were dissolved in 100 mL of diphenylether and refluxed for 2 h. After cooling to room temperature, the precipitate was then filtered several times, washed with petroleum ether, and dried in vacuo.

*General Procedure for N^1-Benzylation of **10a–d**.* First, 20 mmol of the quinolone derivatives **9** were suspended in 10 mL of DMF, 48 mmol of K_2CO_3 and 100 mmol of benzyl chloride were added, and the solution was kept at 80 °C for 20 h. After cooling to room temperature, the surplus of K_2CO_3 was then filtered and the solvents evaporated. The oily residue was crystallized from ethanol and the precipitate collected by filtration and dried in vacuo.

*General Procedure for the Amidation of **11a–c** and **12a–d**.* First, 2.0–5.0 mmol of the corresponding esters **10** were levigated with a 2- or 8-fold surplus of 2-aminobutanol and 4-aminohexanol, respectively, and heated to 150 °C to melt the esters. In the case a solid developed, the mixture was then cooled down and the solid was recrystallized from ethanol. If no solid developed, the mixture was heated for another 6 h. After cooling to room temperature, the obtained precipitate was filtered and recrystallized from ethanol.

*General Procedure for the Conversion of Alcohol to Bromine, Compounds **13a–c** and **14a–d**.* First, 2.0–5.6 mmol of the hydroxyalkyl substituted 4-oxo-quinolinecarboxamides **11** and **12**, respectively, were dissolved in a huge excess of conc HBr. Then a tenth of conc sulfuric acid (of HBr) was carefully added, and the solution was refluxed for 4–6 h. After cooling to room temperature the solution was poured into water. This solution was extracted with chloroform several times. The combined organic phases were neutralized with K_2CO_3 and the solvent evaporated. The so obtained solid was crystallized in ethanol and recrystallized from methanol.

*General Procedure for the Synthesis of the Quinolone-iperoxo Hybrids **2a–c** and **3a–d**.* First, 0.4 mmol of the bromoalkyl 4-oxo-quinoline-3-carboxamides **13**/**14** were dissolved in 20 mL of acetonitrile, and 2–4 equiv of iperoxo-base[43] and a catalytic amount of K_2CO_3 were added. The mixture was then heated to 55 °C in a sealed container. The reaction was followed up by TLC (silica gel, $MeOH/NH_4NO_2$ = 3:2, R_f = 0.54–0.68). When the reaction was completed (after 6–20 days) the mixture was very slowly poured (dropped) into diethyl ether. The so-obtained precipitate was filtered through a frit. The solid was washed with diethyl ether and dried in vacuo. If necessary, the solid precipitate can be recrystallized from methanol.

*6-(Hydroxymethyl)naphthalen-2-ol (**21**).* To a solution of 6-hydroxy-2-naphthoic acid **19** (1 g, 5.32 mmol) in methanol (30 mL) was added 10 drops of 98% sulfuric acid, and the solution was refluxing at 90 °C for 24 h. After the reaction, the solution was concentrated under vacuum and the ester **20** was dissolved in freshly distilled tetrahydrofuran anhydrous (30 mL). The solution was cooled to 0 °C using ice/NaCl bath, and lithium aluminum hydride (350 mg, 9.21 mmol) was added to the above solution portionwise while maintaining the temperature lower than 0 °C. The mixture was then allowed to rise to room temperature gradually and stirred at room temperature for 24 h. The mixture was cooled to less than 10 °C using ice/water bath, and water (30 mL) was added to the mixture dropwise to quench the reaction. The mixture was then extracted with ethyl acetate (3 × 30 mL). The organic phases were combined, dried over sodium sulfate anhydrous, and concentrated under vacuum to get **21** as off-white solid (3.4 g, 74%).

*(6-(3-Chloropropoxy)naphthalen-2-yl)methanol (**22a**).* The mixture of **21** (300 mg, 1.72 mmol), 1-chloro-3-iodopropane (204 μL, 1.90 mmol), sodium hydroxide (40 mg, 1.9 mmol), water (2 mL), and acetonitrile (5 mL) was heated at 65 °C overnight. Ethyl acetate (20 mL) and water (20 mL) were added to the reaction mixture, the organic phase was separated, and the aqueous phase was extracted with (2 × 20 mL) ethyl acetate. The organic phases were combined, dried over sodium sulfate anhydrous, and concentrated under vacuum. The residue was purified via column chromatography using petroleum ether:ethyl acetate 3:1 as eluent system. The target compound **22a** was yielded as yellow solid (310 mg, 72%).

*tert-Butyl((6-(3-chloropropoxy)naphthalen-2-yl)methoxy)-dimethylsilane (**23a**).* To the solution of **22a** (310 mg, 1.2 mmol), triethylamine (258 μL, 1.8 mmol), and catalytic amount of DMAP (15 mg, 0.12 mmol) in diethyl ether (20 mL) was added *tert*-butyldimethylchlorosilane (217 mg, 1.44 mmol), and the mixture was agitated overnight at room temperature. Water (30 mL) and diethyl ether (20 mL) were added to the reaction mixture. The organic phase was separated, and the aqueous phase was extracted with diethyl ether (2 × 20 mL). The organic phases were combined, washed with saturated ammonia chloride solution, dried over sodium sulfate anhydrous, and concentrated under vacuum. The residue was used directly in the next step without further purification.

*(S)-tert-Butyl 4-(3-(6-((tert-Butyldimethylsilyloxy)methyl)-naphthalen-2-yloxy)propyl)-2-ethyl-3-oxo-1-thia-4,8-diazaspiro-[4.5]decane-8-carboxylate (**25a**).* A solution of compound **23a** and sodium iodide (216 mg, 1.44 mmol) in acetone (20 mL) was refluxed overnight. The precipitate was filtered, and the filtrate was concentrated under vacuum to get compound **24a**. To the suspension of sodium hydride (60% in paraffin oil, 86 mg, 2.16 mmol) in dry *N*,*N*′-dimethylformamide (5 mL) under ice/water bath was added compound **18** portionwise (432 mg, 1.44 mmol). The resulting mixture was agitated for 0.5 h. Then the solution of compound **24a** in dry *N*,*N*′-dimethylformamide (5 mL) was added dropwise, and the resulting mixture was allowed to warm to room temperature and stirred overnight. The mixture was concentrated under vacuum. The residue was diluted with ethyl acetate (20 mL) and washed with citric acid 5% aqueous solution (10 mL) and brine (10 mL). The organic phase was separated, dried over sodium sulfate anhydrous, and concentrated under vacuum. The residue was purified via column chromatography using petroleum ether:ethyl acetate 3:1 as eluent system. The target compound was yielded as yellow oil (170 mg, 23% from **22a**).

*(S)-tert-Butyl 2-Ethyl-4-(3-(6-(hydroxymethyl)naphthalen-2-yloxy)propyl)-3-oxo-1-thia-4,8-diazaspiro[4.5]decane-8-carboxylate (**26a**).* To the starting material **25a** (170 mg, 0.27 mmol) was added the mixed solution of acetic acid/water/tetrahydrofuran (3:1:1, 10 mL), and the resulting solution was stirred overnight at room temperature. The solution was then cooled to ≤5 °C with ice/water bath, and the pH value of was regulated to ≥10 with 25% ammonia aqueous solution. Then the mixture was extracted with ethyl acetate (3 × 20 mL). The organic phases were combined, washed with brine, dried over sodium sulfate anhydrous, and concentrated under vacuum. The residue was purified via column chromatography using petroleum ether:ethyl acetate 1:1 as eluent system. The target compound **26a** was yielded as yellow oil (120 mg, 76%).

*(S)-tert-Butyl 2-Ethyl-4-(3-(6-(iodomethyl)naphthalen-2-yloxy)-propyl)-3-oxo-1-thia-4,8-diazaspiro[4.5]decane-8-carboxylate (**27a**).* To the solution of triphenyl phosphine (92 mg, 0.35 mmol) and imidazole (32 mg, 0.47 mmol) in dichloromethane (10 mL) was added iodine (89 mg, 0.35 mmol). The resulting mixture was agitated at room temperature for 1 h. Then the solution of **26a** (120 mg, 0.23 mmol) in dichloromethane (5 mL) was added to the above mixture dropwise, and the mixture was stirred for 1–2 h. The saturated

dx.doi.org/10.1021/jm500860w | J. Med. Chem. XXXX, XXX, XXX–XXX

solution of sodium dithionite (5 mL) was added to the reaction mixture and was agitated vigorously for 10 min. Then water (20 mL) and dichloromethane (20 mL) were added, the organic phase was separated, and the aqueous phase was extracted with dichloromethane (2 × 20 mL). The organic phases were combined, dried over sodium sulfate anhydrous, and concentrated under vacuum. The residue was then purified via column chromatography using petroleum ether:ethyl acetate 3:1 as eluent system to yield the product as yellow oil (90 mg, 62%).

*(S)-tert-Butyl 4-(3-(6-((3-(Ethoxycarbonyl)-8-fluoro-4-oxoquinolin-1(4H)-yl)methyl)naphthalene-2-yloxy)propyl)-2-ethyl-3-oxo-1-thia-4,8-diazaspiro[4.5]decane-8-carboxylate (**28a**).* The mixture of **9a** (21 mg, 0.09 mmol), **27a** (50 mg, 0.08 mmol), and sodium carbonate (13 mg, 0.12 mmol) in DMF (5 mL) was heated to 50 °C and stirred vigorously overnight. Water (20 mL) and ethyl acetate (20 mL) was added to the mixture, and the organic phase was separated. The aqueous phase was extracted with ethyl acetate (2 × 20 mL). The organic phases were combined, dried over sodium sulfate anhydrous, and concentrated under vacuum. The residue was purified via column chromatography (ethyl acetate:methanol, 25:1 as eluent system) to yield the product as yellow oil (20 mg, 34%).

*(S)-Ethyl 1-((6-(3-(2-Ethyl-3-oxo-1-thia-4,8-diazaspiro[4.5]decan-4-yl)propoxy)naphthalen-2-yl)methyl)-8-fluoro-4-oxo-1,4-dihydroquinoline-3-carboxylate (**29a**).* To the solution of **28a** (110 mg, 0.15 mmol) in dichloromethane (5 mL) was added the solution of HCl in diethyl ether (3 mL). The resulting solution was stirred at room temperature for 24 h. The reaction mixture was basified with 25% ammonia solution under ice/water bath until the pH value ≥10. The aqueous phase was extracted with dichloromethane (3 × 30 mL). The organic phases were combined, dried over sodium sulfate anhydrous, and concentrated under vacuum. The residue was purified via column chromatography by using dichloromethane:methanol:ammonia 10:1:0.1 as eluent system. The target compound was obtained (40 mg, 42%) as yellow oil.

Determination of Inertness of Compound 13a toward Glutathione. The buffer used was identical to the one applied in the pharmacological assays, consisting of HBSS (purchased from Life Technologies GmbH) and HEPES (20 mM). Solutions of compound **13a** in DMSO (1 mM) and glutathione in water (1 mM and 0.1 mM) were prepared. Two ratios (1:1 and 10:1 of compound **13a**:glutathione) were investigated. Solutions of compound **13a** (100 μL) and glutathione (100 μL) were added to the buffer (800 μL) to form a solution (1000 μM), with the concentration of **13a** being identical to the highest concentration applied in the pharmacological experiments. The solution was mixed and after 4 h of incubation at 28 °C analyzed by LC-MS (method: water/methanol, 1 mL/min flow rate, gradient 5−90%, 18 min, MS scan 100−1000). No products apart from the starting materials could be detected.

Pharmacology. *Materials and Methods.* Reagents and cell culture media were purchased from Sigma-Aldrich (Taufkirchen, Germany) and Life Technologies (Darmstadt, Germany), and all of the laboratory reagents were from Sigma-Aldrich (Taufkirchen, Germany) unless specified otherwise. Commercially obtained compounds had >99% purity. HEPES was purchased from AppliChem (Darmstadt, Germany), and pertussis toxin (PTX) was purchased from Biotrend (Cologne, Germany). UBO-QIC (FR900359) was kindly provided by Profs. G. M. König and E. Kostenis, University of Bonn. [^{3}H]NMS (specific activity 85.4 Ci/mmol) was purchased from PerkinElmer (Rodgau, Germany). The buffer applied in functional and binding experiments comprised Hank's Balanced Salt Solution (HBSS; Life Technologies, Darmstadt, Germany) with 20 mM HEPES, pH 7.0. Stock solutions of water-soluble compounds were prepared and further diluted in incubation buffer, and poorly water-soluble compounds were prepared in pure DMSO and further diluted in buffer if possible without precipitating. In experiments applying the EPIC system, the final DMSO concentration per well never exceeded 1.3%, as this concentration did not induce a signal of its own; in binding experiments, the highest DMSO concentration applied was 10%. Thus, very poorly soluble compounds such as **33a** were applicable only at a very low concentration of 0.3 μM (cf. Results and Discussion). In the IP1-accumulation assay DMSO concentrations varied between 0.5 and 5%.

Cell Culture. Chinese hamster ovary cells (CHO) stably expressing the hM$_1$ receptor (CHO-hM$_1$ cells) were cultured in Ham's Nutrient Mixture F-12 (HAM- F12) supplemented with 10% (v/v) FCS (FCS), 100 U/mL penicillin, 100 μg/mL streptomycin, 0.2 mg/mL G418, and 2 mM L-glutamine at 37 °C in a 5% CO_2 humidified atmosphere.

Binding Experiments. Radioligand binding experiments using live CHO-hM$_1$ cells were performed in 96-well microtiter plates (ABgene, Germany) applying 75000 cells/well as described previously.[5,19] Experiments were conducted at 28 °C using [^{3}H]NMS as the radioactive probe (2 nM for [^{3}H]NMS dissociation and 0.2 nM for equilibrium binding experiments).[5] Incubation time necessary to reach binding equilibrium was checked by quantification of the retarding action of the compounds on [^{3}H]NMS dissociation; incubation time amounted to 3 h in case of the allosteric moieties **13a** and **14a** and to 8 h in the case of **2a** and **3a**. Radioligand [^{3}H]NMS binding characteristics B_{max} and K_D in live CHO-hM$_1$ cells did not change over 8 h.

Binding experiments addressing the effects of selected test compounds on the inhibition of specific [^{3}H]NMS binding to membranes from CHO-hM$_1$ cells by the endogenous agonist acetylcholine were carried out as described earlier[56] with two differences. First, the incubations were carried out in 10 mM HEPES, 10 mM $MgCl_2$, 100 mM NaCl, and 0.2 mM GTP, pH 7.4, at 30 °C, and second, the analysis of the binding data was independent from a model and based on curving fitting applying a four parameter logistic equation.

Dynamic Mass Redistribution (DMR) Assay. A general protocol has been published recently.[43] DMR assays using live CHO-hM$_1$ cells were carried out as outlined elsewhere.[5] For a chemical "knockout" of selected G proteins, cells were pretreated either with 100 ng/mL PTX for 16−24 h (G_i proteins)[4] or with 1 μM UBO-QIC for 1.5 h (G_q proteins).[57,58]

IP1 Assay. Changes in the concentration of the second messenger IP1 in CHO-hM$_1$ cells were quantified with the HTRF-IP1 kit (Cisbio International) on a Mithras LB 940 plate reader (Berthold Technologies, Bad Wildbad, Germany) according to the manufacturer's instructions and as described previously in detail.[59] In brief, cells were resuspended in assay buffer (HEPES, 10 mM, $CaCl_2$, 1 mM, $MgCl_2$, 0.5 mM, KCl, 4.2 mM, NaCl, 146 mM, glucose, 5.5 mM, and LiCl, 50 mM, pH 7.4) and dispensed in 384-well microplates at a density of 100000 cells/well. After preincubation in assay buffer for 30 min at 37 °C, 5% CO_2, cells were stimulated with the test compounds for 30 min at 37 °C. The reactions were stopped by the addition of 50 mM Na_2HPO_4/KH_2PO_4 phosphate buffer (pH 7.0), 1 mM KF, and 1.25% Triton X-100 containing HTRF assay reagents. The assay was incubated 60 min at room temperature, and time-resolved FRET signals were measured after excitation at 320 nm using the Mithras LB 940 multimode plate reader. Data analysis was based on the fluorescence ratio emitted by labeled IP1 (665 nm) over the light emitted by the europium cryptate-labeled anti-IP1 (620 nm). Levels of IP1 were normalized to the amount generated in the presence 100 μM acetylcholine.

Data Analysis. Data analysis in general was performed using Prism 5.03 (GraphPad Software, San Diego, CA). [^{3}H]NMS equilibrium binding data from homologous inhibition curves applying CHO-hM$_1$ cells, and the effect on DMR of all compounds listed in Table 1 were analyzed by a four-parameter logistic function. The resulting IC_{50} values from [^{3}H]NMS homologous inhibition data were used to calculate equilibrium dissociation constants K_D according to De Blasi et al.[60] Data from [^{3}H]NMS dissociation experiments in the absence and in the presence of test compounds were analyzed as described recently.[56] All DMR responses were solvent-corrected. The quantification of probe-induced DMR signals was based on the signal value (upward- or downward-deflected) at 2400 s and normalized on the corresponding value elicited by ACh (100 μM), which was set at 100%. Concentration−effect curves of DMR measurements in the presence of ACh, iperoxo, and pilocarpine were fitted to the operational model of agonism.[50] In the analyses applying the

dx.doi.org/10.1021/jm500860w | J. Med. Chem. XXXX, XXX, XXX−XXX

operational model, the parameter E_{max}, i.e., the maximum response of the system, was defined and constrained to the effect observed in the presence of 100 μM ACh, $E_{max,ACh}$ = constant = 100%; the parameter *basal*, i.e., the basal response of the system, was defined and constrained to the response in the absence of ACh, $basal_{ACh}$ = constant = 0%. The gobal fits provided parameter estimates of K_A and τ to reflect functional affinity and efficacy of the agonists, respectively.

The concentration−effect curves of hybrid-induced DMR were analyzed according to the operational model of agonism for dynamic ligands as recently described by Bock et al.[30]

$$E = \frac{E_{max}}{1 + \frac{([AB] + K_D)^{n_{op}}}{[AB]^{n_{op}} \cdot \tau_{dyn}^{n_{op}}}} \quad (1)$$

E_{MAX} denotes the maximum response of the system defined as the maximum effect in the presence of a saturating concentration of ACh. *AB* is the concentration of the dynamic ligand. τ_{dyn} represents the dynamic transduction coefficient of the ligand. n_{op} indicates the transducer slope. K_D indicates the functional affinity of the ligand *AB* determined with functional data and can be expressed as[30]

$$K_D = \frac{K_A \cdot K_B}{K_A + K_B} \quad (2)$$

K_A and K_B are taken to reflect the affinity of the ligand AB for the active pose and for the inactive receptor binding pose, respectively.[30]

Global Fitting Analysis. To simultaneously quantify the active and inactive ligand binding poses of each of the dynamic ligands **2a**, **3a** using both binding *and* functional data, we, on the basis of the mathematical framework pubished recently,[30] applied a new unbiased global fitting approach to four different sets of concentration−effect curves (CECs) for each dynamic ligand: (CEC 1) functional change in DMR induced by the reference agonist acetylcholine, (CEC 2) functional change in DMR induced by the dynamic ligands **2a** or **3a**, (CEC 3) [^{3}H]NMS displacement by the dynamic ligands **2a** or **3a**, and (CEC 4) [^{3}H]NMS displacement by the corresponding allosteric moieties **13a** or **14a**, respectively.

The global fits of every set of four curves was performed using the following equations: Concentration−effect curves of the dynamic ligands **2a** or **3a** (CEC 2) together with the reference agonist acetylcholine (CEC 1) were fitted using eq 3 (derived from replacing K_D in eq 1 with eq 2)

$$E = \frac{E_{max}}{1 + \frac{\left([AB] + \frac{K_A \cdot K_B}{K_A + K_B}\right)^{n_{op}}}{[AB]^{n_{op}} \cdot \tau_{dyn}^{n_{op}}}} \quad (3)$$

[^{3}H]NMS equilibrium binding data (CEC 3) of the dynamic ligands **2a** or **3a** were analyzed according to a model of bivalent ligand binding to the orthosteric and allosteric site (i.e., an extended allosteric ternary complex model)[4,30,61] and attributed to the following equation:

$$Y = \frac{[L_{hybrin}] \cdot R_T}{[L_{hybrin}] + K_L \cdot \frac{\left(1 + [AB] \cdot \left(\frac{K_A + K_B}{K_A \cdot K_B}\right)\right)}{\left(1 + \frac{\alpha'_{hybr} \cdot [AB]}{K_B}\right)}} \quad (4)$$

Y is the specific binding of the radioligand L [i.e., [^{3}H]NMS]. $[L_{hybrin}]$ indicates the concentration of the radioligand L, R_T is the total number of receptors. K_L denotes the equilibrium dissociation constant of the [^{3}H]NMS−receptor complex and represents the affinity of the radioligand L. *AB* is the concentration of the dynamic ligand **2a** or **3a**. K_A and K_B are the equilibrium dissociation constants of the active and inactive dynamic ligand−receptor complexes, respectively. They are considered to represent the affinities of the dynamic ligand in the active and inactive pose, respectively. α'_{hybr} denotes the cooperativity between *L* and *AB*, and positive cooperativity is reflected by $\alpha' > 1$. Equation 4 has been previously applied to fit binding data of bipharmacophoric, dualsteric ligands.[4,5,30] To reduce the number of variables during global curve fitting, R_T in eq 4 was replaced by B_0*(K_L + L_{hybrin})/L_{hybrin}; B_0 indicates the specific equilibrium binding of a fixed radioligand concentration in the absence of the dynamic ligand *AB*.

As the final component of the global fit, [^{3}H]NMS equilibrium binding data (CEC 4) of the allosteric moieties **13a** or **14a** were analyzed according to the allosteric ternary complex model[4,30,61] and attributed to the following equation:[62]

$$Y = B_0 \frac{(1 + K_L \cdot [L_{fragin}])(1 + \alpha'_{frag} \cdot (K_B \cdot [B])^{n_{frag}})}{1 + (K_B \cdot [B])^{n_{frag}} + K_L \cdot [L_{fragin}](1 + \alpha'_{frag} \cdot (K_B \cdot [B])^{n_{frag}})} \quad (5)$$

B_0 indicates the specific equilibrium binding of a fixed radioligand concentration in the absence of the allosteric moiety *B*, K_L is the equilibrium dissociation constant of the radioligand [^{3}H]NMS, K_B is the equilibrium dissociation constant of the allosteric moieties **13a** or **14a** at the free receptor, and α'_{frag} is the cooperativity factor of the interaction between the allosteric moiety B and the radioligand L. $[L_{fragin}]$ indicates the concentration of the radioligand [^{3}H]NMS in the equilibrium binding experiments characterizing the allosteric fragments, and n_{frag} is a slope factor describing the steepness of the curve. In the case of **13a** and **14a**, for which the slope factors of the [^{3}H]NMS equilibrium binding curves were significantly different from unity (Figure 5B,D), eq 5, as had already been reported,[62] does not express interactions that can be visualized by a molecular scheme. Therefore, to analyze these data under conditions in which the mechanical implications are clear, the global analyses were also carried out with slope factors n_{frag} constrained to unity (Supporting Information, Figure 7B,D). For the sake of consistency throughout the global analysis, the equilibrium association constants K_B and K_L from the original equation[62] were treated as equilibrium dissociation constants by replacing them with $K_B = 1/K_B$ and $K_L = 1/K_L$, respectively.

Overall, global fitting yielded the parameter values K_A, K_B, τ_{dyn}, n_{op} (transducer slope of eq 1), α'_{hybr}, α'_{frag}, and n_{frag} (slope of eq 5). Two versions of the global fit procedure were applied. In both cases, the parameters L_{hybrin}, L_{fragin}, K_L, and B_0 were constrained to fixed values, and K_A and K_B were always treated as shared variables. In the first version of the global fit (cf. Table 2 and Figure 5), the parameter values α'_{hybr}, α'_{frag}, and n_{frag} (slope of eq 5) were treated as individual variables. In contrast, in the second version of the global fit (cf. Supporting Information, Table 2 and Figure 7A,C), the parameters α'_{hybr} and α'_{frag} were additionally treated as shared variables and n_{frag} was constrained to unity.

To further ramify the mechanism of partial agonism of **2a** and **3a**, a separate global fit was applied to the data sets of the dynamic ligands **2a** and **3a**. In this regard, τ_{dyn} in eq 3 was further resolved to[30]

$$\tau_{dyn} = \tau_{max} \cdot \frac{K_B}{K_A + K_B} = \frac{\varepsilon_{max} \cdot R_T}{K_E} \cdot \frac{K_B}{K_A + K_B} \quad (6)$$

τ_{dyn} is the dynamic transduction coefficient of the ligand and can be expressed as the product of τ_{max}, the maximum transduction coefficient of the dynamic ligand at 100% occupancy of receptors in the active pose and the fraction of the ligand−receptor complexes in the active pose ($K_B/K_A + K_B$). τ_{max} is defined by the system-independent maximum intrinsic efficacy of the dynamic ligand ε_{max} and a system-dependent part R_T/K_E. R_T is the total number of receptors. K_E indicates the level of stimulus that elicits the half maximal system response. Replacing τ_{dyn} in eq 3 with eq 6 yielded:

$$E = \frac{E_{max}}{1 + \frac{\left([AB] + \frac{K_A \cdot K_B}{K_A + K_B}\right)^{n_{op}}}{[AB]^{n_{op}} \cdot \left(\frac{\varepsilon_{max} \cdot R_T}{K_E} \cdot \frac{K_B}{K_A + K_B}\right)^{n_{op}}}} \quad (7)$$

During global fitting of the **2a**/**13a** and **3a**/**14a** data sets, R_T/K_E was treated as single variable and taken to represent the receptor reserve; ε_{max} and n_{op} were treated as variables (further details, cf. text and Table 2 and Supporting Information, Table 1). In global fits, K_A and K_B were treated as shared variables and R_T/K_E set constant to unity allowing

dx.doi.org/10.1021/jm500860w | J. Med. Chem. XXXX, XXX, XXX−XXX

estimation of ε_{max}* (equivalent to τ_{max} in the absence of a receptor reserve).

Estimation of Fractional Occupancy. The set of occupancy curves of **2a** and **3a**, depicted in parts C and E of Figure 5, respectively, were calculated as described previously.[30] In brief, we used the following equations from the Supporting Information, Note 1 of ref 30: eq 7 for the total binding of a dynamic ligand, eq 12 for its fractional occupancy in the active pose, and eq 14 for the fractional occupancy in the inactive pose. Equations 7, 12, and 14 from Supporting Information, Note 1 in ref 30 were set up and used in a single user-defined equation in Prism 5.03 (GraphPad Software, San Diego, CA); with known numerical estimates of K_A, K_B, and R_T, obtained as a result of the global analysis of CECs (1−4), see above, the software was then able to calculate and draw simultaneously the occupancy curves for the three binding situations shown.

R_{pose}, the ratio of the active and inactive receptor binding pose was calculated as previously reported:[30]

$$R_{pose} = -\log\left(\frac{K_A}{K_B}\right) = -\log\left(\frac{K_{active}}{K_{inactive}}\right) \quad (8)$$

and implemented into the global fit as a transform to report. The software was able to report either the corresponding standard errors (Table 2, Supporting Information, Tables 1 and 2) or the 95% confidence intervals (Figure 5F and Supporting Information, Figure 7F).

Statistical Analysis. Experimental data are presented as means ± SEM of N observations. Single comparisons were performed using Student's t-test and multiple comparisons using One-Way ANOVA with Newman−Keuls multiple comparison test. Nonlinear regression data analyses based on different models were compared by a F-test. In all cases, $P < 0.05$ (*) was considered as the level of statistical significance, $P < 0.01$ (**) and $P < 0.001$ (***) was indicated for selected comparisons.

■ ASSOCIATED CONTENT

Supporting Information

More detailed synthetic procedures of intermediates as well as compound structure characterization. This material is available free of charge via the Internet at http://pubs.acs.org.

■ AUTHOR INFORMATION

Corresponding Authors

*For M.D.: phone, 0049-931-3189676; E-mail, michael.decker@uni-wuerzburg.de.
*For U.H.: phone, 0049-931-3185461; E-mail, u.holzgrabe@pharmazie.uni-wuerzburg.de.
*For C.T.: phone, 0049-228-739104; E-mail, traenkle@uni-bonn.de.

Author Contributions

The manuscript was written through contributions of all authors. All authors have given approval to the final version of the manuscript. X.C., J.K., and J.H. contributed equally. M.D., U.H., and C.T. conceived the project. X.C. designed and synthesized compounds **4a**,**b** and **5a**−**c**. J.K. performed the syntheses of compounds **2a**−**c** and **3a**−**d**. J.H. conducted DMR and IP1 assays, all of the binding experiments in live CHO-hM$_1$ cells and membranes, analyzed data, and contributed to the discussion. C.Z. and W.S. conducted DMR assays, and R.S. conducted DMR and IP1 assays. A.B. provided important ideas. K.M. and A.B. contributed to the discussion. C.T. developed and applied the global curve fitting procedure, allowing to analyze simultaneously functional and binding data with the mathematical framework for dynamic ligands, which had been published recently.[30]

Notes

The authors declare no competing financial interest.

■ ACKNOWLEDGMENTS

We gratefully acknowledge the financial support by the Deutsche Forschungsgemeinschaft given to U.H. (HO 1368/12-1), M.D. (DE 1546/4-1), and K.M. (MO 821/2-1). We thank Corning Inc. for their support on the Epic system and Professor E. Kostenis for allowing us to perform measurements with it. The skillful technical assistance of Mechthild Kepe and Iris Jusen is gratefully acknowledged.

■ ABBREVIATIONS USED

Aβ, β-amyloid protein; ACh, acetylcholine; AD, Alzheimer's disease; BQCA, benzyl quinolone carboxylic acid; BQCAd, BQCA derived compound; CHO, Chinese hamster ovary cell; EC, extracellular loops; DMR, dynamic mass redistribution; GPCRs, G-protein coupled receptors; M$_1$, muscarinic acetylcholine subtype 1; NMDA, *N*-methyl-D-aspartate; NMS, *N*-methylscopolamine; PAM, positive allosteric modulator; Pilo, pilocarpine; PTX, pertussis toxin; SARs, structure−activity relationships; TBPBd, TBPB derived compound; TM, transmembrane helix; QNB, quinuclidinyl benzilate

■ REFERENCES

(1) Mohr, K.; Tränkle, C.; Kostenis, E.; Barocelli, E.; De Amici, M.; Holzgrabe, U. Rational design of dualsteric GPCR ligands: Quests and promise. *Br. J. Pharmacol.* **2010**, *159*, 997−1008.
(2) Davie, B. J.; Christopoulos, A.; Scammells, P. J. Development of M1 mAChR allosteric and bitopic ligands: prospective therapeutics for the treatment of cognitive deficits. *ACS Chem. Neurosci.* **2013**, *17*, 1026−1048.
(3) Steinfeld, T.; Mammen, M.; Smith, J. A.; Wilson, R. D.; Jasper, J. R. A novel multivalent ligand that bridges the allosteric and orthosteric binding sites of the M2 muscarinic receptor. *Mol. Pharmacol.* **2007**, *72*, 291−302.
(4) Antony, J.; Kellershohn, K.; Mohr-Andrae, M.; Kebig, A.; Prilla, S.; Muth, M.; Heller, E.; Disingrini, T.; Dallanoce, C.; Bertoni, S.; Schrobang, J.; Tränkle, C.; Kostenis, E.; Christopoulos, A.; Hoeltje, H.-D.; Barocelli, E.; De Amici, M.; Holzgrabe, U.; Mohr, K. Dualsteric GPCR targeting: a novel route to binding and signaling pathway selectivity. *FASEB J.* **2009**, *23*, 442−450.
(5) Bock, A.; Merten, N.; Schrage, R.; Dallanoce, C.; Bätz, J.; Klöckner, J.; Schmitz, J.; Matera, C.; Simon, K.; Kebig, A.; Peters, L.; Müller, A.; Schrobang-Ley, J.; Tränkle, C.; Hoffmann, C.; De Amici, M.; Holzgrabe, U.; Kostenis, E.; Mohr, K. The allosteric vestibule of a seven transmembrance helical receptor controls G-Protein coupling. *Nature Commun.* **2012**, *3*, 1044 DOI: 10.1038/ncomms2028.
(6) Lane, J. R.; Sexton, P. M.; Christopoulos, A. Bridging the gap: bitopic ligands of G-protein-coupled receptors. *Trends Pharmacol. Sci.* **2013**, *34*, 59−66.
(7) Bock, A.; Mohr, K. Dualsteric GPCR targeting and functional selectivity: the paradigmatic M(2) muscarinic acetylcholine receptor. *Drug Discovery Today: Technol.* **2013**, *10*, 245−252.
(8) Bymaster, F. P.; McKinzie, D. L.; Felder, C. C.; Wess, J. Use of M1−M5 muscarinic receptor knockout mice as novel tools to declineate the physiological roles of the muscarinice cholinergic system. *Neurochem. Res.* **2003**, *28*, 437−442.
(9) Lanzafame, A. A.; Christopoulos, A.; Mitchelson, F. Cellular signaling mechanisms for muscarinic acetylcholine receptors. *Recept. Channels* **2003**, *9*, 241−260.
(10) Fisher, A. M1 muscarinic agonists target major hallmarks of Alzheimer's disease—the pivotal role of brain M1 receptor. *Neurodegener. Dis.* **2008**, *5*, 237−240.
(11) Liu, L.; Zhao, R.; Bai, Y.; Stanish, L. F.; Evans, J. E.; Sanderson, M. J.; Bonventre, J. V.; Rittenhouse, A. R. M1 muscarinic receptors

inhibit L-type Ca^{2+} current and M-current by divergent signal transduction cascades. *J. Neurosci.* **2006**, *26*, 11588−11598.
(12) Marino, M. J.; Rouse, S. T.; Levey, A. I.; Potter, L. T.; Conn, P. J. Activation of the genetically defined M1 muscarinic receptor potentiates *N*-methyl-D-aspartate (NMDA) receptor currents in hippocampal pyramidal cells. *Proc. Natl. Acad. Sci. U. S. A.* **1998**, *95*, 11465−11470.
(13) Fisher, A. Cholinergic treatments with emphasis on M1 muscarinic agonists as potential disease-modifying agents for Alzheimer's disease. *Neurotherapeutics* **2008**, *5*, 433−442.
(14) Decker, M.; Holzgrabe, U. M_1 muscarinic acetylcholine receptor allosteric modulators as potential therapeutic opportunities for treating Alzheimer's disease. *Med. Chem. Commun.* **2012**, *3*, 752−762.
(15) Anagnostaras, S. G.; Murphy, G. G.; Hamilton, S. E.; Mitchell, S. L.; Rahnama, N. P.; Nathanson, N. M.; Silva, A. J. Selective cognitive dysfunction in acetylcholine M1 muscarinic receptor mutant mice. *Nature Neurosci.* **2003**, *6*, 51−58.
(16) Kruse, A. C.; Hu, J.; Pan, A. C.; Arlow, D. H.; Rosenbaum, D. M.; Rosemond, E.; Green, H. F.; Liu, T.; Chae, P. S.; Dror, R. O.; Shaw, D. E.; Weis, W. I.; Wess, J.; Kobilka, B. K. Structure and dynamics of the M3 muscarinic acetylcholine receptor. *Nature* **2012**, *482*, 552−556.
(17) Haga, K.; Kruse, A. C.; Asada, H.; Yurugi-Kobayashi, T.; Shiroishi, M.; Zhang, C.; Weis, W. I.; Okada, T.; Kobilka, B. K.; Haga, T.; Kobayashi, T. Structure of the human M2 muscarinic acetylcholine receptor bound to an antagonist. *Nature* **2012**, *482*, 547−551.
(18) Kruse, A. C.; Ring, A. M.; Manglik, A.; Hu, J.; Hu, K.; Eitel, K.; Hübner, H.; Pardon, E.; Valant, C.; Sexton, P. M.; Christopoulos, A.; Felder, C. C.; Gmeiner, P.; Steyaert, J.; Weis, W. I.; Garcia, K. C.; Wess, J.; Kobilka, B. K. Activation and allosteric modulation of a muscarinic acetylcholine receptor. *Nature* **2013**, *504*, 101−106.
(19) Schrage, R.; Seemann, W. K.; Klöckner, J.; Dallanoce, C.; Racké, K.; Kostenis, E.; De Amici, M.; Holzgrabe, U.; Mohr, K. Agonists with supraphysiological efficacy at the muscarinic M2 ACh receptor. *Br. J. Pharmacol.* **2013**, *169*, 357−370.
(20) Venkatakrishnan, A. J.; Deupi, X.; Lebon, G.; Tate, C. G.; Schertler, G. F.; Babu, M. M. Molecular signatures of G-protein-coupled receptors. *Nature* **2013**, *494*, 185−194.
(21) Hulme, E. C.; Birdsall, N. J.; Buckley, N. J. Muscarinic receptor subtypes. *Annu. Rev. Pharmacol. Toxicol.* **1990**, *30*, 633−673.
(22) Daval, S. B.; Valant, C.; Bonnet, D.; Kellenberger, E.; Hibert, M.; Galzi, J. L.; Ilien, B. Fluorescent derivatives of AC-42 to probe bitopic orthosteric/allosteric binding mechanisms on muscarinic M1 receptors. *J. Med. Chem.* **2012**, *55*, 2125−2143.
(23) Daval, S. B.; Kellenberger, E.; Bonnet, D.; Utard, V.; Galzi, J. L.; Ilien, B. Exploration of the orthosteric/allosteric interface in human m1 muscarinic receptors by bitopic fluorescent ligands. *Mol. Pharmacol.* **2013**, *84*, 71−85.
(24) Goodwin, J. A.; Hulme, E. C.; Langmead, C. J.; Tehan, B. G. Roof and floor of the muscarinic binding pocket: variations in the binding modes of orthosteric ligands. *Mol. Pharmacol.* **2007**, *72*, 1484−1496.
(25) Gnagey, A. L.; Seldenberg, M.; Ellis, J. Site-directed mutagenesis reveals two epitopes involved in the subtype selectivity of the allosteric interactions of gallamine at muscarinic acetylcholine receptors. *Mol. Pharmacol.* **1999**, *56*, 1245−1253.
(26) Dror, R. O.; Green, H. F.; Valant, C.; Borhani, D. W.; Valcourt, J. R.; Pan, A. C.; Arlow, D. H.; Canals, M.; Lane, J. R.; Rahmani, R.; Baell, J. B.; Sexton, P. M.; Christopoulos, A.; Shaw, D. E. Structural basis for modulation of a G-protein-coupled receptor by allosteric drugs. *Nature* **2013**, *503*, 295−299.
(27) Lazareno, S.; Popham, A.; Birdsall, N. J. M. Allosteric interactions of staurosporine and other indolocarbazoles with *N*-[methyl-^{3}H]scopolamine and acetylcholine at muscarinic receptor subtypes: identification of a second allosteric site. *Mol. Pharmacol.* **2000**, *58*, 194−207.
(28) Lazareno, S.; Popham, A.; Birdsall, N. J. M. Analogs of WIN 62,577 define a second allosteric site on muscarinic receptors. *Mol. Pharmacol.* **2002**, *62*, 1492−1505.
(29) Matera, C.; Flammini, L.; Quadri, M.; Vivo, V.; Ballabeni, V.; Holzgrabe, U.; Mohr, K.; De Amici, M.; Barocelli, E.; Bertoni, S.; Dallanoce, C. Bis(ammonio)alkane-type agonists of muscarinic acetylcholine receptors: synthesis, in vitro functional characterization, and in vivo evaluation of their analgesic activity. *Eur. J. Med. Chem.* **2014**, *75*, 222−232.
(30) Bock, A.; Chirinda, B.; Krebs, F.; Messerer, R.; Bätz, J.; Muth, M.; Dallanoce, C.; Klingenthal, D.; Tränkle, C.; Hoffmann, C.; De Amici, M.; Holzgrabe, U.; Kostenis, E.; Mohr, K. Dynamic ligand binding dictates partial agonism at a G protein-coupled receptor. *Nature Chem. Biol.* **2014**, *10*, 18−20.
(31) January, B.; Seibold, A.; Whaley, B.; Hipkin, R. W.; Lin, D.; Schonbrunn, A.; Barber, R.; Clark, R. B. Beta2-adrenergic receptor desensitization, internalization, and phosphorylation in response to full and partial agonists. *J. Biol. Chem.* **1997**, *272*, 23871−23879.
(32) Mailman, R. B.; Murthy, V. Third generation antipsychotic drugs: partial agonism or receptor functional selectivity? *Curr. Pharm. Des.* **2010**, *16*, 488−501.
(33) Kuduk, S. D.; Beshore, D. C. Novel M(1) allosteric ligands: a patent review. *Expert Opin. Ther. Pat.* **2012**, *22*, 1385−1398.
(34) Mistry, S. N.; Valant, C.; Sexton, P. M.; Capuano, B.; Christopoulos, A.; Scammells, P. J. Synthesis and pharmacological profiling of analogues of benzyl quinolone carboxylic acid (BQCA) as allosteric modulators of the M_1 muscarinic receptor. *J. Med. Chem.* **2013**, *56*, 5151−5172.
(35) Yeatman, H. R.; Lane, J. R.; Choy, K. H.; Lambert, N. A.; Sexton, P. M.; Christopoulos, A.; Canals, M. Allosteric modulation of M1 muscarinic acetylcholine receptor internalization and subcellular trafficking. *J. Biol. Chem.* **2014**, *289*, 15856−15866.
(36) Ma, L.; Seager, M. A.; Wittmann, M.; Jacobson, M.; Bickerl, D.; Burno, M.; Jones, K.; Graufelds, V. K.; Xu, G.; Pearson, M.; McCampbell, A.; Gaspar, R.; Shughrue, P.; Danziger, A.; Regan, C.; Flick, R.; Pascarella, D.; Garson, S.; Doran, S.; Kreatsoulas, C.; Veng, L.; Lindsley, C. W.; Shipe, W.; Kuduk, S.; Sur, C.; Kinney, G.; Seabrook, G. R.; Ray, W. J. Selective activation of the M_1 muscarinic acetylcholine receptor achieved by allosteric potentiation. *Proc. Natl. Acad. Sci. U. S. A.* **2009**, *106*, 15950−15955.
(37) Shirey, J. K.; Brady, A. E.; Jones, P. J.; Davis, A. A.; Bridges, T. M.; Kennedy, J. P.; Jadhav, S. B.; Menon, U. N.; Xiang, Z.; Watson, M. L.; Christian, E. P.; Doherty, J. J.; Quirk, M. C.; Snyder, D. H.; Lah, J. J.; Levey, A. I.; Nicolle, M. M.; Lindsley, C. W.; Conn, P. J. A selective allosteric potentiator of the M_1 muscarinic acetylcholine receptor increases activity of medial prefrontal cortical neurons and restores impairments in reversal learning. *J. Neurosci.* **2009**, *29*, 14271−14286.
(38) Abdul-Ridha, A.; López, L.; Keov, P.; Thal, D. M.; Mistry, S. N.; Sexton, P. M.; Lane, J. R.; Canals, M.; Christopoulos, A. Molecular determinants of allosteric modulation at the M1 muscarinic acetylcholine receptor. *J. Biol. Chem.* **2014**, *289*, 6067−6079.
(39) Fisher, A.; Bar-Ner, N.; Karton, Y. Methods and compositions for treatment of central and peripheral nervous system disorders and novel compounds useful therefor. U.S. Patent 7,439,251, 2008.
(40) Kuduk, S. D.; Chang, R. K.; Di Marco, C. N.; Ray, W. J.; Ma, L.; Wittmann, M.; Seager, S. A.; Koeplinger, K. A.; Thompson, C. D.; Hartman, G. D.; Bilodeau, M. T. Quinolizidinone carboxylic acids as CNS penetrant, selective M_1 allosteric muscarinic receptor modulators. *ACS Med. Chem. Lett.* **2010**, *1*, 263−267.
(41) Fisher, A. Cholinergic modulation of amyloid precursor protein processing with emphasis on M1 muscarinic receptor: Perspective and challenges in treatment of Alzheimer's disease. *J. Neurochem.* **2012**, *120* (Suppl 1), 22−33.
(42) Schröder, R.; Janssen, N.; Schmidt, J.; Kebig, A.; Merten, N.; Hennen, S.; Müller, A.; Blättermann, S.; Mohr-Andrä, M.; Zahn, S.; Wenzel, J.; Smith, N. J.; Gomeza, J.; Drewke, C.; Milligan, G.; Mohr, K.; Kostenis, E. Deconvolution of complex G protein-coupled receptor signaling in live cells using dynamic mass redistribution measurements. *Nature Biotechnol.* **2010**, *28*, 943−949.
(43) Schröder, R.; Schmidt, J.; Blättermann, S.; Peters, L.; Janssen, N.; Grundmann, M.; Seemann, W.; Kaufel, D.; Merten, N.; Drewke, C.; Gomeza, J.; Milligan, G.; Mohr, K.; Kostenis, E. Applying label-free

dynamic mass redistribution technology to frame signaling of G-protein-coupled receptors noninvasively in living cells. *Nature Protoc.* **2011**, *6*, 1748−1760.
(44) Leyva, E.; Monreal, E.; Hernández, A. Synthesis of fluoro-4-hydroxyquinoline-3-carboxylic acids by the Gould−Jacobs reaction. *J. Fluor. Chem.* **1999**, *94*, 7−10.
(45) Klöckner, J.; Schmitz, J.; Holzgrabe, U. Convergent, short synthesis of the muscarinic superagonist iperoxo. *Tetrahedron Lett.* **2010**, *51*, 3470−3472.
(46) Walz, A. J.; Miller, M. J. Synthesis and biological activity of hydroxamic acid-derived vasopeptidase inhibitor analogues. *Org. Lett.* **2002**, *4*, 2047−2050.
(47) Zhu, S.-F.; Song, X.-G.; Li, Y.; Cai, Y.; Zhou, Q.-L. Enantioselective copper-catalyzed intramolecular O−H insertion: an efficient approach to chiral 2-carboxy cyclic ethers. *J. Am. Chem. Soc.* **2010**, *132*, 16374−16376.
(48) Nair, S. K.; Matthews, J. J.; Stephan, J. C.; Ma, C.; Dovalsantos, E. Z.; Grubbs, A. W.; Sach, N. W.; ten Hoeve, W.; Koster, H.; Flahive, E. J.; Tanis, S. P.; Renner, M.; van Wiltenburg, J. Novel synthesis of CP-734432, an EP4 agonist, using Sharpless asymmetric dihydroxylation. *Tetrahedron Lett.* **2010**, *51*, 1451−1454.
(49) Henning, R.; Lattrell, R.; Hermann, J. G.; Leven, M. Synthesis and neuroleptic activity of a series of 1-[1-(benzo-1,4-dioxan-2-ylmethyl)-4-piperidinyl]benzimidazolone derivatives. *J. Med. Chem.* **1987**, *30*, 814−819.
(50) Black, J. W.; Leff, P. Operational models of pharmacological agonism. *Proc. R. Soc. London B: Biol. Sci.* **1983**, *220*, 141−162.
(51) Lazareno, S.; Birdsall, N. J. M. Detection, quantitation, and verification of allosteric interactions of agents with labeled and unlabeled ligands at G-protein-coupled receptors: Interaction of strychnine and acetylcholine at muscarinic receptors. *Mol. Pharmacol.* **1995**, *48*, 362−378.
(52) Jakubík, J.; Bacáková, L.; El-Fakahany, E. E.; Tuček, S. Positive cooperativity of acetylcholine and other agonists with allosteric ligands on muscarinic acetylcholine receptors. *Mol. Pharmacol.* **1997**, *52*, 172−179.
(53) De Amici, M.; Dallanoce, C.; Holzgrabe, U.; Tränkle, C.; Mohr, K. Allosteric ligands for G protein-coupled receptors: a novel strategy with attractive therapeutic opportunities. *Med. Res. Rev.* **2010**, *30*, 463−549.
(54) Bock, A.; Kostenis, E.; Tränkle, C.; Lohse, M. J.; Mohr, K. Pilot the pulse: controlling the multiplicity of receptor dynamics. *Trends Pharmacol. Sci.* **2014**, *35*, 630−638.
(55) De la Cruz, A.; Elguero, J.; Goya, P.; Martínez, A. Tautomerism and Acidity in 4-Quinolone-3-carboxylic Acid Derivatives. *Tetrahedron* **1992**, *29*, 6135−6150.
(56) Fang, L.; Jumpertz, S.; Zhang, Y.; Appenroth, D.; Fleck, C.; Mohr, K.; Tränkle, C.; Decker, M. Hybrid molecules from xanomeline and tacrine: enhanced tacrine actions on cholinesterases and muscarinic M1 receptor. *J. Med. Chem.* **2010**, *53*, 2094−2103.
(57) Nesterov, A.; Hong, M.; Hertel, C.; Jiao, P.; Brownell, L.; Cannon, E. Screening a plant extract library for inhibitors of cholecystokinin receptor CCK1 pathways. *J. Biomol. Screening* **2010**, *15*, 518−527.
(58) Hennen, S.; Wang, H.; Peters, L.; Merten, N.; Simon, K.; Spinrath, A.; Blättermann, S.; Akkari, R.; Schrage, R.; Schröder, R.; Schulz, D.; Vermeiren, C.; Zimmermann, K.; Kehraus, S.; Drewke, C.; Pfeifer, A.; König, G. M.; Mohr, K.; Gillard, M.; Müller, C. E.; Lu, Q. R.; Gomeza, J.; Kostenis, E. Decoding signaling and function of the orphan G protein-coupled receptor GPR17 with a small-molecule agonist. *Sci. Signaling* **2013**, *6*, ra93 DOI: 10.1126/scisignal.2004350.
(59) Schröder, R.; Merten, N.; Mathiesen, J. M.; Martini, L.; Kruljac-Letunic, A.; Krop, F.; Blaukat, A.; Fang, Y.; Tran, E.; Ulven, T.; Drewke, C.; Whistler, J.; Pardo, L.; Gomeza, J.; Kostenis, E. The C-terminal tail of CRTH2 is a key molecular determinant that constrains Galphai and downstream signaling cascade activation. *J. Biol. Chem.* **2009**, *284*, 1324−1336.
(60) De Blasi, A.; O'reilly, K.; Motulsky, H. J. Calculating receptor number from binding experiments using same compound as radioligand and competitor. *Trends Pharmacol. Sci.* **1989**, *10*, 227−229.
(61) May, L. T.; Leach, K.; Sexton, P. M.; Christopoulos, A. Allosteric modulation of G protein-coupled receptors. *Annu. Rev. Pharmacol. Toxicol.* **2007**, *47*, 1−51.
(62) Tränkle, C.; Weyand, O.; Voigtländer, U.; Mynett, A.; Lazareno, S.; Birdsall, N. J.; Mohr, K. Interactions of orthosteric and allosteric ligands with [3H]dimethyl-W84 at the common allosteric site of muscarinic M2 receptors. *Mol. Pharmacol.* **2003**, *64*, 180−190.